Cellular and Molecular Life Sciences (2023) 80:87
https://doi.org/10.1007/s00018-023-04722-x

ORIGINAL ARTICLE

A Rab10–ACAP1–Arf6 GTPases cascade modulates M4 muscarinic acetylcholine receptor trafficking and signaling

Rongmei Xu[1] · Min Wan[1,2] · Xuemeng Shi[1,3] · Shumin Ma[1] · Lina Zhang[1] · Ping Yi[1] · Rongying Zhang[1]

Received: 27 November 2022 / Revised: 6 February 2023 / Accepted: 8 February 2023 / Published online: 14 March 2023

Abstract

Membrane trafficking processes regulate the G protein-coupled receptor activity. The muscarinic acetylcholine receptors (mAChRs) are highly pursued drug targets for neurological diseases, but the cellular machineries that control the trafficking of these receptors remain largely elusive. Here, we revealed the role of the small GTPase Rab10 as a negative regulator for the post-activation trafficking of M4 mAChR and the underlying mechanism. We show that constitutively active Rab10 arrests the receptor within Rab5-positive early endosomes and significantly hinders the resensitization of M4-mediated Ca^{2+} signaling. Mechanistically, M4 binds to Rab10-GTP, which requires the motif ^{386}RKKRQMAA^{393} (R^{386}-A^{393}) within the third intracellular loop. Moreover, Rab10-GTP inactivates Arf6 by recruiting the Arf6 GTPase-activating protein, ACAP1. Strikingly, deletion of the motif R^{386}-A^{393} causes M4 to bypass the control by Rab10 and switch to the Rab4-facilitated fast recycling pathway, thus reusing the receptor. Therefore, Rab10 couples the cargo sorting and membrane trafficking regulation through cycle between GTP-bound and GDP-bound state. Our findings suggest a model that Rab10 binds to the M4 like a molecular brake and controls the receptor's transport through endosomes, thus modulating the signaling, and this regulation is specific among the mAChR subtypes.

Keywords GPCR · Muscarinic acetylcholine receptors · Protein sorting · Endosomal recycling · Rab4 · Signaling

Abbreviations

AD	Alzheimer's disease
A568-Tf	Alexa568-labeled Transferrin
Arf6	ADP-ribosylation factor 6
β_1AR	β_1 Adrenoceptor
CCh	Carbachol
CDE	Clathrin-dependent endocytic
CHC	Clathrin heavy chain
CHX	Cycloheximide
CIE	Clathrin-independent endocytic
Co-IP	Co-immunoprecipitation
DOPr	δ-Opioid receptor
EE	Early endosome
EHBP-1	Effector EH domain binding protein 1
ER	Endoplasmic reticulum
FI	Fluorescence intensity
GGA3	Golgi-associated, gamma adaptin ear-containing, Arf-binding protein 3
GIPC	$G\alpha_i$-interacting protein C terminus
GPCR	G protein-coupled receptor
GST	Glutathione S-transferase
GST-GGA3-PBD	Protein 3 binding domain (PBD) of GGA3 fused to glutathione S-transferase
mAChRs	Muscarinic acetylcholine receptors
LHR	Luteinizing hormone receptor
PBD	Protein 3 binding domain
PDZ	Postsynaptic density-95/Discs large/Zonula occludens 1
PM	Plasma membrane
PTX	Pertussis toxin
RE	Recycling endosome
SNX27	Sorting nexin 27

✉ Ping Yi
pingy@hust.edu.cn

✉ Rongying Zhang
ryzhang@mail.hust.edu.cn

[1] Key Laboratory of Molecular Biophysics of the Ministry of Education, College of Life Science and Technology, Huazhong University of Science and Technology, Wuhan, Hubei, China

[2] Present Address: Department of Molecular Biology and Genetics, Cornell University, Ithaca, USA

[3] Present Address: College of Life Science, Henan Agricultural University, Zhengzhou, Henan, China

TAC	IL-2 receptor α-chain
TfR	Transferrin receptor
TLR4	Toll-like receptor 4
WT	Wild type

Introduction

G protein-coupled receptors (GPCRs) constitute the largest superfamily of cell surface signaling proteins and are the therapeutic targets of approximately one-third of the drugs on the market [1]. For most GPCRs, the plasma membrane (PM) is the most important functional destination where they bind to their respective ligands and activate cognate heterotrimeric G proteins, arrestins, and other signaling proteins that in turn activate downstream effectors [2]. GPCR activation often leads to increased internalization and redistribution of receptors from the PM to the interior of cells [3]. The resultant decrease in PM receptor density desensitizes the cells to further ligand stimulation. Some GPCRs are internalized and delivered to lysosomes for degradation, in which case resensitization to further ligand stimulation requires synthesis of new receptors [4]. Other GPCRs are recycled to the PM, and the intracellular dwell time varies among recycled GPCRs [5, 6]. Therefore, the post-activation trafficking of GPCRs significantly contributes to the biological effects of GPCRs. Altering receptor trafficking will profoundly reprogram GPCR signal transduction and physiologically represents a mechanism for cells to adapt to dynamic extracellular milieu [7].

The early endosome (EE) is classically considered as the primary sorting compartment for all internalized cargoes. For many years, it was thought that the default pathway, a sort of passive diffusion into endosome tubules, was sufficient to explain receptor recycling [8]. However, recent studies have identified "recycling sequences" acted by the postsynaptic density-95/Discs large/Zonula occludens 1 (PDZ) ligand in the C-terminal tails of many GPCRs, such as β_1 adrenoceptor (β_1AR), β_2AR, luteinizing hormone receptor (LHR), and mGluR5, etc. [9–13]. By recognizing these linear sequences, the PDZ domain-containing proteins, such as sorting nexin 27 (SNX27), Gα_i-interacting protein C terminus (GIPC), or Na^+/H^+ exchanger regulatory factor, cause the internalized receptors to be recycled from spatially and biochemically distinct tubular microdomains in the endosomes [12, 14, 15]. Although several studies have reported that non-PDZ sequences exist in other GPCRs and promote efficient recycling of the internalized receptor, how these sequences functionally facilitate receptors to be sorted into distinct endosomal tubules remain largely elusive [10, 16]. Undoubtedly, research to address these questions is the important challenge in the field of GPCR cell biology.

Muscarinic acetylcholine receptors (mAChRs) belong to the rhodopsin-like class A family of GPCRs, are extensively distributed in the central and peripheral nervous system, and control vital physiological activities. Among the five subtypes of mAChRs, M1, M3, and M5 classically signal through $G_{q/11}$ proteins to mediate the excitatory neuromodulatory actions of ACh, whereas M2 and M4 signal through $G_{i/o}$ proteins to mediate the inhibitory neuromodulatory actions of ACh [17]. Disturbances of cholinergic signaling have been implicated in many pathological conditions including Alzheimer's disease (AD) and schizophrenia [18]. M4 mAChR has attracted particular attention for the treatment of these neurological disorders [19, 20]. The agonist-activated M4 has been shown to internalize in clathrin/β-arrestin-dependent manner and traffic to Rab11-positive recycling endosomes (REs) before finally returning to the PM [17, 21, 22]. Nevertheless, the cytoplasmic C-terminus of the M4 does not contain the PDZ ligand sequence, implying that it is sorted to the PM probably not mediated by SNX27 or other PDZ-containing proteins [23]. The molecular machines driving M4 sorting and trafficking from the EEs remain to be fully elucidated.

Rab family small GTPases are well-known master regulators of intracellular membrane traffic by cycling between a GDP-bound inactive state and a GTP-bound active state [24, 25]. Accumulating evidence shows that these small GTPases are capable of regulating the trafficking and signaling of GPCRs through their physical and specific association with the receptors [26–28]. Among over 60 mammalian Rab members, Rab10 is unique due to its multiple subcellular localizations, including the endoplasmic reticulum (ER), Golgi/TGN, the endosomes/phagosomes, and the primary cilia [25, 29]. Accordingly, it preforms various functions, from the biosynthetic secretory pathway to the post-endocytic endosomal trafficking processes. Using a knockin mouse model and proteomic analyses, Jade et al. reported that Rab10 regulates the cell-surface delivery of δ-opioid receptor (DOPr), as it does for the Toll-like receptor 4 (TLR4) and GLUT4 [27, 30, 31]. Meanwhile, studies on the *C. elegans* have revealed that Rab10 appears to promote actin binding and endosomal tubulation by cooperating with the effector EH domain-binding protein 1 (EHBP-1) [32]. However, it remains to identify the extent to which Rab10 influences physiologically or pathologically meaningful cargo proteins for their post-endocytic transport. Here, our interest is focused on the yet underexplored role of Rab10 in the intracellular trafficking of GPCRs.

In the present study, we aim to explore the role of small GTPase Rabs in particular sequence-driven GPCR endosomal sorting and trafficking. We discovered that constitutively active Rab10 stalls the transport of agonist-activated M4 mainly on Rab5-positive EEs. Mechanistically, GTP-bound Rab10 binds the M4, which requires the motif R^{386}-A^{393}

near the C-terminal end of the ICL3. Further, Rab10 forms GTPase cascade with Arf6 to control membrane trafficking through the recycling pathway. Our findings imply that manipulating Rab10 provides a new way to understand better the regulation of M4 receptor post-endocytic trafficking and the signaling afterward. In addition, these findings provide a fresh perspective on the development and treatment of M4-associated neurological disorders.

Materials and methods

Cell culture and transfection

Human embryonic kidney-derived (HEK) 293 cells were grown in high glucose DMEM (Gibco) and Chinese hamster ovary-K1 (CHO-K1) cells were cultured in Ham's F-12 medium (Gibco), supplemented with 10% (*v*/*v*) fetal bovine serum, 100 U/ml penicillin and 100 µg/ml streptomycin at 37 °C in a humidified atmosphere containing 5% CO_2. Transient transfections were performed using Lipofectamine 2000 (Invitrogen) following the manufacturer's instructions, and experiments were performed 24 h post-transfection. Unless otherwise stated, 0.4 µg fluorescent protein (FP)-tagged Rab10 variant encoding plasmid was added in 12-well to ensure low-expression level of various FP-Rab10. For short hairpin RNA (shRNA) interference experiment, knockdown efficiency and subsequent experiments were performed after 72 h post-transfection.

DNA constructs

Plasmids encoding EGFP-tagged M4 and i3 loop-based deletion mutants, HA-EGFP-M4, HA-EGFP-M4 ΔR^{386}-A^{393}, and shCHC were already described [33]. EGFP-tagged M1, M3, and M5 were generated by replacing M4 with M1, M3, and M5. All mCherry and EGFP-tagged plasmids were constructed by subcloning individual cDNA into the pmCherry-C3 and pEGFP-C1 vector at specific restriction enzyme digestion sites. HA-ACAP1 was generated by modifying Flag-ACAP1 (gift from Prof. Victor Hsu, Brigham and Women's Hospital, Department of Medicine, Harvard Medical School, Boston, MA 02115, USA) with HA epitope (YPYDVPDYA), which was produced by the PCR overlap extension method. All FP-tagged Arf6 variant encoding plasmids were constructed by inserting Arf6 and FP cDNAs into pcDNA3.1 vector. To constructs the shRab10-RFP and shAS160-RFP plasmids, the nucleotide target sequence of the human *Rab10* gene (5′-GCTGAAGATATCCTTCGAAAG-3′) [34] and *AS160* gene (5′-GACCTAAACTGCAACCCTA-3′) [35] were inserted into pRNAT-H1.1-shutter/RFP vector. Unless stated otherwise, all mutations in this study were generated using site-directed mutagenesis. All constructs were verified by DNA sequencing. The cDNAs, plasmids, and primers used in our study are listed in Supplementary Table S1.

Reagents

Alexa 568-conjugated transferrin (A568-Tf, T23365) was purchased from Invitrogen. Carbachol (CCh, 51-83-2) and digitonin (D141-100MG) were purchased from Sigma and cycloheximide (CHX, 66-81-9) was purchased from Aladdin. Fluo-4 AM was purchased from Thermo Fisher Scientific (F14202). Pertussis Toxin was purchased from Merck Millipore (PTX, 516560).

Quantitative real-time polymerase chain reaction (qRT-PCR)

RNA extraction was performed with RNA-easy isolation Reagent (R701-01, Vazyme). The complementary DNA (cDNA) synthesis was carried out using the Reverse Transcription Kit (BL696A, Biosharp). All real-time PCRs were performed using Bio-Rad CFX96 Touch Real-Time PCR Detection System with SYBR Green Real-time PCR Master Mix (QPK-201, TOYOBO). Relative gene expression was analyzed using the $2^{-\Delta\Delta Ct}$ method, and glyceraldehyde-3-phosphate dehydrogenase (*GAPDH*) was used as internal control.

Receptor internalization and recycling

For the internalization assay, transfected HEK293 cells were incubated with 100 µM CCh in serum-free medium (α-MEM without phenol red supplemented with 20 mM Hepes pH 7.4 and 0.1% BSA) at 37 °C for various periods of time. Cells were then washed extensively with ice-cold serum-free medium and fixed with 3.7% paraformaldehyde for 15 min at room temperature. To analyze receptor recycling, transfected HEK293 cells were pre-incubated in 20 µg/ml CHX-containing medium for 30 min and then treated with 100 µM CCh in CHX-containing medium for 60 min; after extensive ice-cold wash, cells were incubated in CHX-containing fresh medium at 37 °C for indicated periods of time. Receptor internalization and recycling were examined using confocal microscope.

Enzyme-linked immunosorbent assay (ELISA)

Detection of HA-tagged M4 receptors at the cell surface by ELISA was performed. Briefly, HEK-293 cells were co-transfected with HA-tagged M4 and Rab10, Arf6 or ACAP1 and seeded into 96-well microplates. After CCh treatment

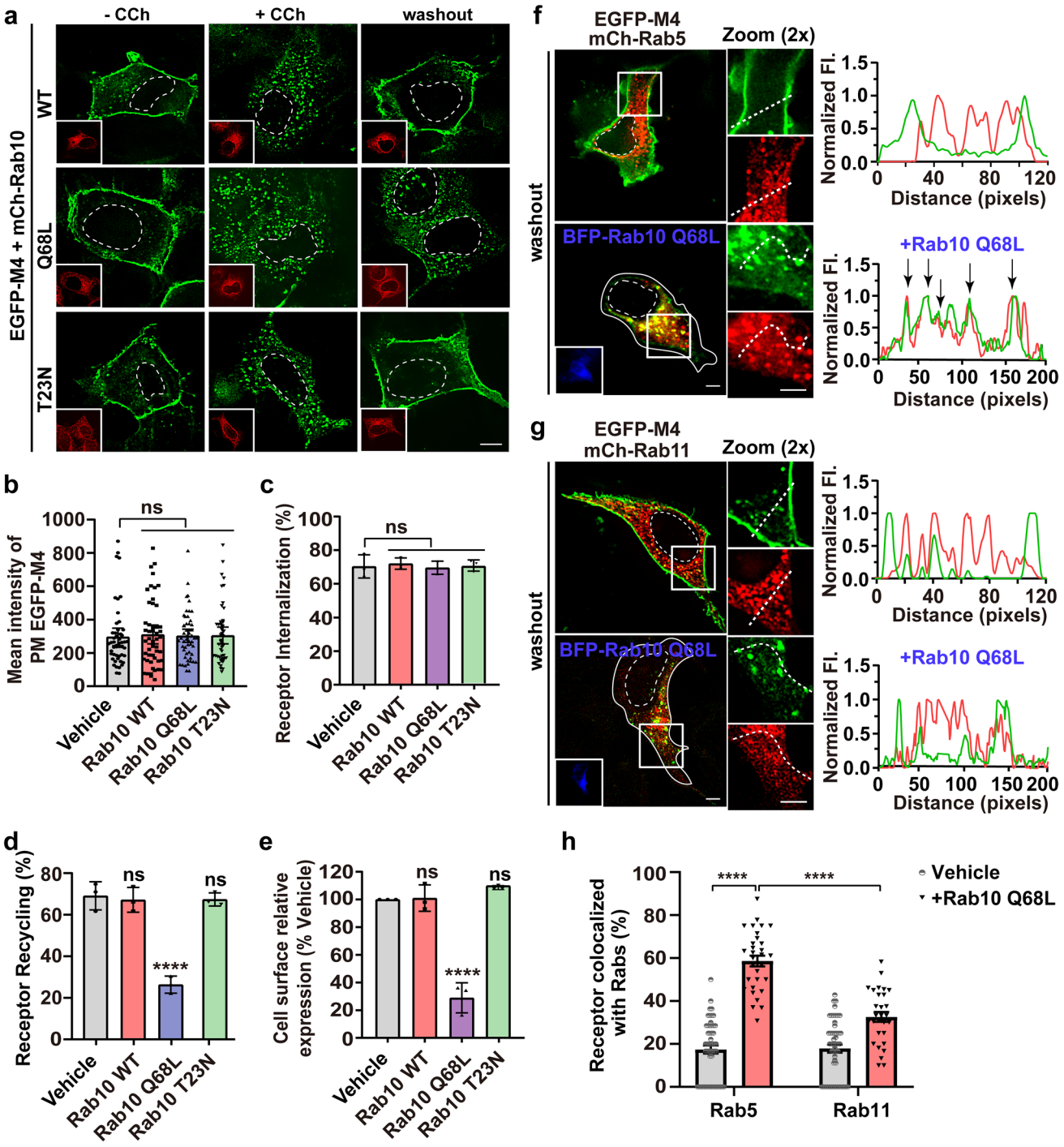

for 60 min followed by washout 60 min in CHX-containing warm media, cells were fixed with 3.7% paraformaldehyde and blocked with 1% BSA. HA-tag was detected with a monoclonal rat anti-HA antibody coupled with horseradish peroxidase (Roche, Indianapolis, USA). Bound antibodies were detected by chemiluminescence using SuperSignal substrate (Thermo Fisher Scientific) and luminescence was measured using a luminescence microplate reader (Tecan).

A568-Tf recycling assay

Transfected HEK293 cells were incubated with 10 µg/ml A568-Tf for 30 min at 4 °C. Unbound A568-Tf was removed by washing three times with ice-cold PBS. Thereafter, cells were chased in complete medium at 37 °C for 0, 5, 30, and 60 min, respectively, followed by washing three times with ice-cold PBS and fixed with 3.7% paraformaldehyde in PBS

◂**Fig. 1** Rab10 Q68L causes the agonist-activated M4 receptor retention in the Rab5-positive EEs. **a** Representative confocal micrographs showing the PM localization (−CCh), internalization (+CCh), and recycling of EGFP-M4 (washout) affected by the expression of mCherry-tagged wild type, Q68L, or T23N Rab10. Transfected HEK293 cells were untreated or treated with CCh for 15 min or pretreated with CCh for 60 min followed by 60 min washout. Insets show the expression of individual Rab10 variants. Scale bar, 10 µm. **b–d** Quantification of surface expression level (**b**), internalization (**c**), or recycling efficiency (**d**) of EGFP-M4 in each condition indicated in (**a**), empty vector was co-expressed as vehicle group. Data are displayed as mean ± SEM, $n \geq 30$ cells from three independent experiments in (**b**), and represent mean ± SD from 3 independent experiments in (**c** and **d**). Kruskal–Wallis test with Dunn's post hoc test (**b**) and one-way ANOVA followed by Dunn's post hoc test (**c** and **d**). *ns* not significant; ****$p < 0.0001$. **e** Quantification of the recycling efficiency of HA-tagged M4 receptors using ELISA. HEK293 cells co-expressing Rab10 variants or empty vector were treated with CCh and followed by washout procedure. Data are presented as the percentage of the cell surface M4 expression level compared with vehicle group and shown as mean ± SD from three independent experiments. One-way ANOVA followed by Dunn's post hoc test, *ns* not significant; ****$p < 0.0001$. **f** and **g** Representative confocal micrographs showing Rab10 Q68L effect on the internalized M4 distribution to structures positive for Rab5 (**f**) or Rab11 (**g**) after removal of CCh. Insets show the expression of BFP-Rab10 Q68L. Fluorescence intensity profiles are shown on the right for the indicated region and path. Scale bars, 5 µm. **h** Quantification of M4 colocalization with mCh-Rab5 in (**f**) or mCh-Rab11 in (**g**). Data are displayed as mean ± SEM. $n \geq 30$ cells from three independent experiments. ****$p < 0.0001$ from a two-way ANOVA followed by Tukey's post hoc test. Nuclear boundaries are demarcated with dashed lines. Cell boundaries in (**f** and **g**) are demarcated with solid lines

for 15 min. A568-Tf recycling was examined using confocal microscope.

Digitonin permeabilization

Digitonin permeabilization was used to remove free cytosolic proteins in some experiments. Briefly, cells were washed three times with KHM buffer (20 mM HEPES, 110 mM potassium acetate, and 2 mM magnesium acetate, PH 7.4) and incubated with 50 µg/ml digitonin in KHM buffer for 5 min at RT. Afterwards, the cells were washed three times with KHM buffer to ensure removal of digitonin and fixed with 3.7% paraformaldehyde for 10 min at RT before further execution of experiments.

Western blotting and Co-IP

The standard procedure of Western blotting was described previously [36]. For co-IP, the cell lysates were incubated with primary antibodies overnight at 4 °C, and then incubated with 50% (*v*/*v*) protein G-agarose (16-266, EMD Millipore Corp, USA) for 4 h at 4 °C. The immunoprecipitated proteins were eluted with 2 × Laemmli sample buffer (125 mM Tris, PH 6.8, 20% glycerol, 4% SDS, 0.005% Bromophenol blue, 5% beta-mercaptoethanol) and analyzed by Western blot. Primary and secondary antibodies utilized for Western blot analysis and co-IP are listed in Supplementary Table S2.

Arf6 activation assay

Arf6 activity was measured using an Arf6 Pull-Down Activation Assay Biochem kit (BK033-S; Cytoskeleton), according to the manufacturer's instruction. Briefly, transfected HEK293 cells were lysed on ice for 10 min with lysis buffer. Cell lysates were clarified by centrifugation at 10,000*g* for 2 min and then incubated with GGA3 beads for 1 h at 4 °C. The beads were washed twice with wash buffer. GTPγS (final concentration 200 µM) and GDP (final concentration 1 mM)-treated samples were used as positive and negative controls, respectively. The proteins bound to the beads were eluted with 2 × Laemmli sample buffer and analyzed by Western blot.

Membrane fractionation assay

Transfected HEK293 cells grown on 10-cm-diameter culture plates were washed with ice-cold PBS and harvested in 500 µl of ice-cold homogenization buffer (20 mM Hepes, PH 7.4, 250 mM sucrose and 1 × protease inhibitor cocktail (Roche)). A 25-gauge needle was used to lyse cells, and lysates were centrifuged at 1000 *g* for 10 min at 4 °C to pellet unbroken cells and nuclei. The supernatant was further ultra-centrifuged at 60,000 rpm for 1 h at 4 °C in a TLA 100.1 rotor (Beckman Coulter) to yield a pellet of total cellular membranes and supernatant representing the cytosolic fraction. Pellets were resuspended in SDS lysis buffer (50 mM Tris, 1% SDS, 50 mM DTT, 1 mM PMSF and 1 × protease inhibitor cocktail (Roche)). Equal fractions of cytosol and membrane were analyzed by Western blot. Bands were quantified using ImageJ.

Immunofluorescence (IF)

Transfected cells grown on coverslips were fixed with 3.7% paraformaldehyde, blocked, and permeabilized with 2% BSA and 0.1% saponin, then incubated with 1st antibody for 45 min and 2nd antibody for 45 min at RT. Afterwards, coverslips were mounted onto slides for fluorescence imaging. Primary and secondary antibodies utilized are listed in Supplementary Table S2.

Confocal microscopy

Images were taken using a spinning-disk confocal system (CSU-X1 Nipkow; Yokogawa) equipped with an EM CCD camera (DU897K; ANDOR iXon) and oil objectives (60 × N.A. 1.45, 100 × N.A. 1.3 or 150 × N.A. 1.45). Three

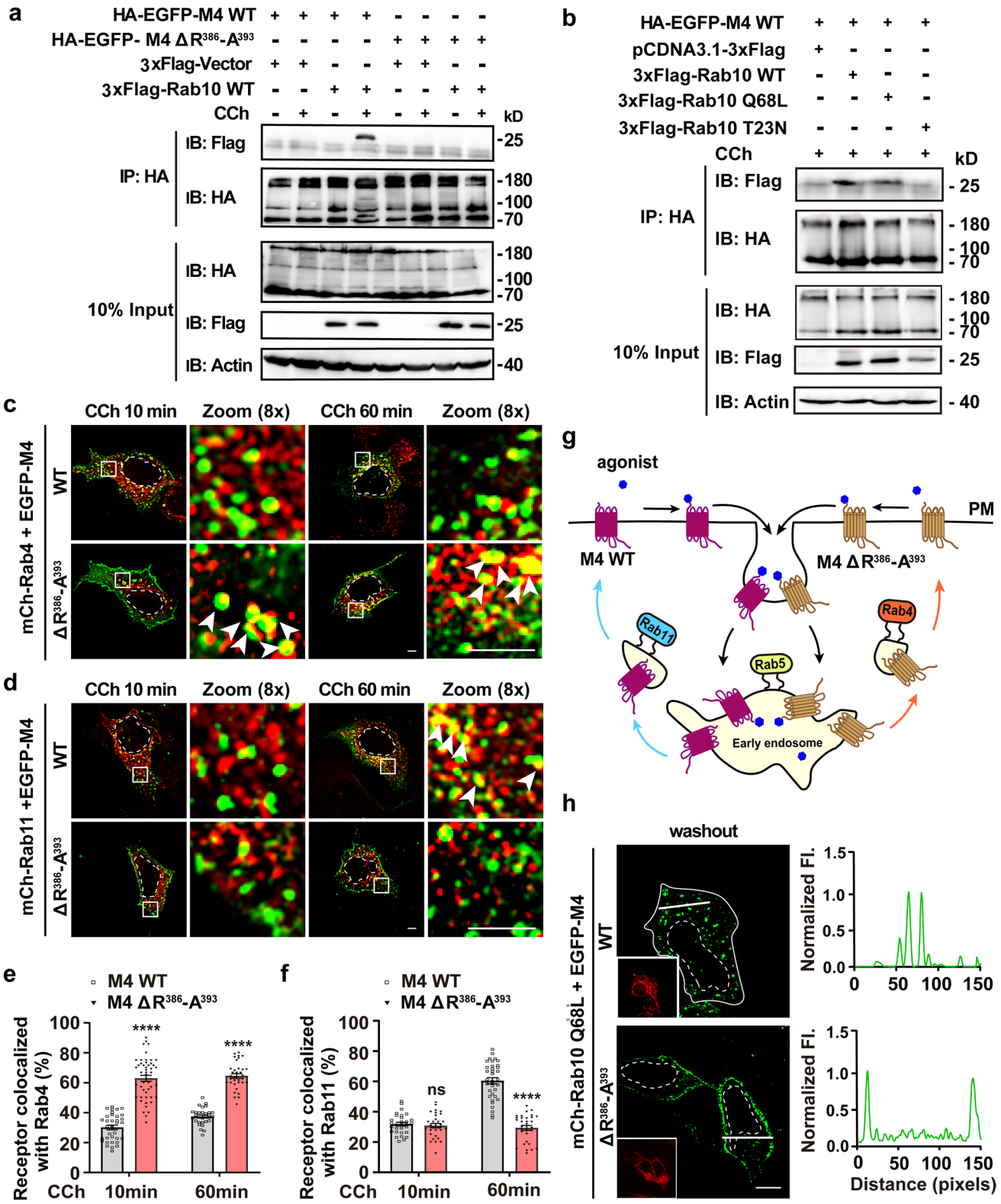

50 mW solid state lasers (491 nm, 561 nm and 405 nm) coupled with an acoustic-optical tunable filter (AOTF) were used to excite GFP, RFP and BFP, respectively. Z-series of optical sections were acquired using a 0.2 μm step size.

For live-cell imaging of M4 receptor internalization, transfected cells were seeded on 25-mm cover glasses (72225-01, Electron Microscopy Sciences). Before imaging, the medium was changed to live-cell imaging buffer

◂**Fig. 2** R^{386}-A^{393} motif is essential for M4 binding to Rab10 and sorting on endosomes. **a** R^{386}-A^{393} motif is necessary for the agonist-activated M4 receptor binding to Rab10. HEK293 cells co-expressing HA-EGFP-M4 or HA-EGFP-M4 ΔR^{386}-A^{393} and 3×Flag-Rab10 or 3×Flag-empty vectors were stimulated with CCh for 60 min or not. Lysates were immunoprecipitated (IP) through the HA epitope followed by immunoblotting using anti-Flag and anti-HA antibodies. Bands with different molecular mass might represent the monomer and oligomers of M4 receptor. **b** Representative co-IP of HA-EGFP-M4 and 3×Flag-Rab10 variants pretreated with CCh for 60 min. Lysates were IP through the HA epitope followed by immunoblotting using anti-Flag and anti-HA antibodies. **c** and **d** Representative confocal micrographs showing the colocalization of M4 WT/ΔR^{386}-A^{393} mutant receptors with mCh-Rab4 (**c**) or mCh-Rab11 (**d**) upon brief (10-min) or prolonged (60-min) stimulation of CCh. Scale bars, 5 μm. **e** and **f** Colocalization of WT or mutant M4 receptor with Rab4 (**e**) or Rab11 (**f**) was calculated for each condition as depicted in (**c**) and (**d**). Data are displayed as mean ± SEM. $n \geq 30$ cells from three independent experiments. Mann–Whitney test. *ns* not significant; ****$p < 0.0001$. **g** Schematic showing after agonist-activation and internalization into Rab5-EEs, M4 WT is sorted into Rab11-REs and M4 ΔR^{386}-A^{393} mutant enters Rab4-EEs for subsequent return to the PM. **h** Confocal micrographs showing the divergent impact of Rab10 Q68L expression on the recycling of WT and ΔR^{386}-A^{393} M4 receptors. Cells were co-transfected with EGFP-M4 WT/ΔR^{386}-A^{393} constructs and mCherry-Rab10 Q68L. Insets show the expression of Rab10 Q68L. Fluorescence intensity profiles are shown on the right for the indicated path. Scale bar, 10 μm. Nuclear boundaries are demarcated with dashed lines. Cell boundaries in (**h**) are demarcated with solid lines

(α-MEM supplemented with 20 mM HEPES, pH 7.4 and 10% FBS). Cells were then placed on the microscope stage and maintained in a dark atmosphere-controlled chamber at 37 °C and 5% CO_2. Upon CCh addition, images were acquired for 15 min with exposure time of about 300 ms at 1 s interval. For live-cell imaging of M4 recycling, transfected cells were pre-stimulated with CCh for 45 min, and then chased at 37 °C in CHX-containing fresh medium. Images were acquired 15 min post-chasing at 1 s interval.

Live-cell Ca^{2+} imaging

RFP-M4-expressing CHO-K1 cells were seeded at a 1:1 ratio with plain cells on 25-mm cover glasses for 12 h and then loaded with 1 μM Fluo-4-AM in Flex buffer (130 mM NaCl, 5.1 mM KCl, 0.42 mM KH_2PO4, 0.32 mM Na_2HPO_4, 5.27 mM Glucose, 20 mM HEPES, 3.3 mM Na_2CO_3, 0.1% BSA, 2.5 mM probenecid, pH 7.4) for 1 h. After a brief wash and changing to live-cell imaging buffer, cells were placed on the microscope stage under controlled environmental conditions (37 °C, 5% CO_2). The optimal visual field was determined through the fluorescence of RFP-M4 from the red channel, and Fluo-4-based Ca^{2+} signal was collected at 1 s interval through exciting at 491 nm and emitting at 525 nm. CCh was added in the imaging medium with a final concentration of 100 μM 30 s after baseline recording, and imaging continued for 300 s. For PTX treatment, cells were incubated in 100 ng/ml PTX-containing medium for 12 h at 37 °C and subsequently loaded with Fluo-4 AM as described above. For resensitization examination, prior to Fluo-4 AM loading, cells were treated with 20 μg/ml CHX for 30 min followed by 100 μM CCh stimulation to induce receptors internalization for 15 min. After extensive ice-cold wash, cells were incubated in CHX-containing Flex buffer at 37 °C for 60 min to load Fluo-4-AM. The average intracellular fluorescence intensity of Fluo-4 was analyzed using ImageJ. Intracellular Ca^{2+} flux was calculated using the F to F_0 ratio, according to the equation: FI (fold to basal) $= F/F_0$, where F is the frame-by-frame FI of the selected cells after CCh addition and F_0 is the average FI of selected cells calculated according to frames prior to CCh addition.

Imaging processing and analysis

Images were collected using Andor IQ 3.3 software and 3D deconvolved using AutoQuant X2 (Media Cybernetics) software. Brightness and contrast were adjusted for images in ImageJ 1.52f (Wayne Rasband, National Institutes of Health). A 1.0-pixel-wide median filter and 50-pixel-wide rolling-ball background subtraction were used to increase the signal-to-noise ratio. To determine the average FI of the PM-associated receptor, a 10-pixel-wide line segment was drawn along the contour of the cell using the ImageJ plugin "Selection Brush Tool". The percentage of receptor internalization was calculated according to the formula $\%\text{internalization} = \left(FI_{untreated} - FI_{(CCh,15min)}\right)/FI_{untreated}$, where $FI_{untreated}$ is the average FI along the PM before agonist addition and $FI_{(CCh,15min)}$ is the FI along the PM 15 min after CCh addition. The percentage of receptor recycling was calculated according to $\%\text{recycling} = \left(FI_{(washout,60min)} - FI_{(CCh,60min)}\right) / \left(FI_{untreated} - FI_{(CCh,60min)}\right)$, where $FI_{(CCh,60min)}$ is the average FI along the PM 60 min after CCh addition and $FI_{(washout,60min)}$ is the average FI along the PM 60 min after CCh addition followed by subsequent chasing in CHX-containing fresh medium for 60 min. The statistical results were obtained from the mean of three independent experiments. Linear profile and dot profile analysis for cells were performed using ImageJ plugin "Plot Profile" and "dotted line", respectively. Colocalization analysis was done using ImageJ plugin "JACoP". The percentage of overlapped area between EGFP-M4 and Arf6 variants signals was determined by Manders' coefficient. Colocalization between ACAP1 and Arf6 or Rab10 variants was determined by Pearson's coefficient. For colocalization, the percentage between EGFP-M4 and Rabs signals was scored as the ratio of green puncta signals that were positive for red signals out of the total number of green puncta.

Table 1 Endocytosis and recycling profiles of M4 mutants

M4 mutants	Endocytosis		Recycling
	Clathrin dependence	Arf6 dependence	Arf6 dependence
M4 WT	+ + +, yes	Not	+ + +, yes
M4 ΔV^{373}-A^{393}	+, /	/	/
M4 ΔV^{373}-V^{385}	+ + +, yes	Not	+ + +, yes
M4 ΔR^{386}-A^{393}	+ +, not	Not	+ + +, not

+ + +/+ +/+: the extent of endocytosis or recycling is strong/moderate/mild; /: no detection

Statistical analysis

Statistical analyses were performed using the GraphPad Prism software version 8.0 (GraphPad Software, La Jolla, CA, USA). Significant differences between two groups were carried by unpaired two-tailed Student's *t* test. One-way ANOVA or two-way ANOVA was used to compare multiple groups. Statistical details are shown in figure legends. The following *p* value conventions are used throughout the paper: ns (not significant), $p > 0.05$; $*p < 0.05$; $**p < 0.01$; $***p < 0.001$; $****p < 0.0001$.

Results

Aberrantly activated Rab10 impedes recycling of the agonist-internalized M4 receptor

Previously, we developed N-terminal fluorophore-tagged M4 and M2 mAChRs to visualize their internalization [33]. As seen, most of the exogenously expressed M4 receptors resided at the HEK293 cell surface, similar to the endogenous distribution in PC12 and NG108-15 cells [22, 33]. Following agonist (carbachol, CCh) stimulation, the PM-localized EGFP-M4 signals were substantially diminished and accumulated inside the cells time-dependently, corresponding to agonist-promoted endocytosis (Fig. S1a, b; Video 1). In addition, in line with earlier results [22, 37], a brief CCh stimulation of 15 min caused M4 receptors to be transported into Rab5-positive EEs (59.53%); prolonged stimulation of 60 min, however, promoted the majority of the M4 receptors further transport into Rab11-positive REs (58.99%; Fig. S1c–e). The trafficking fate of internalized M4 receptors upon removal of the agonist was also examined. EGFP-M4-expressing HEK293 cells were treated with CCh for 60 min and followed by a 60-min washout in the fresh medium. As seen, most of the internalized EGFP-M4 molecules recycle back to the PM (Fig. S1a). To ensure that the prominent EGFP-M4 fluorescent intensity build-up along the PM was not due to neosynthesized EGFP-M4 replenishment, cells were co-treated with cycloheximide (CHX) [38], a translation inhibitor. Live-cell imaging further demonstrated that the processes of M4 uptake into the cytosol and recycling back toward the PM are fairly dynamic and effective (Fig. S1b, f; Video 1 and Video 2). In line with the earlier studies [21, 33], knockdown of the expression of clathrin heavy chain (CHC) strongly inhibited the internalization of M4 receptor (Fig. S1g). These results demonstrated that the agonist-activated M4 receptor is internalized through the clathrin-dependent endocytic (CDE) pathway, then enters EEs, and returns to the PM via the Rab11-positive slow recycling pathway. These data also indicated that the fluorophore-tagged M4 mAChR construct is suitable for imaging-based analysis of M4 receptor internalization and recycling, because it is compatible with earlier results obtained by radio-ligand binding assay [17].

No role of Rab10 in post-endocytic GPCR trafficking has ever been reported. Therefore, we investigated the effect of Rab10 on M4 mAChR. First, we determined that the surface expression level of EGFP-M4 in HEK293 cells is unaffected by the co-expressing Rab10 wild type (WT), GTP-locked constitutively active mutant Q68L, or GDP-locked dominant-negative mutant T23N (Fig. 1a, b) [39]. A low-expression transfection strategy for mCherry-rab10 variant plasmids, as verified by the mRNA level (Fig S2a), was used in this study unless otherwise stated. Further, the internalization of the PM-localized M4 molecules upon CCh stimulation in each condition is as effective as that in the vehicle cells, indicating that the aberrant Rab10 GTPase cycle does not obstruct the endocytosis of the agonist-activated M4 receptors (Fig. 1a, c). Curiously, in contrast to Rab10 WT and Rab10 T23N, the co-expression of Rab10 Q68L severely hindered the internalized M4 recycling back to the PM (Fig. 1a, d; 26.41% for Q68L vs. 67.15% and 66.92% for WT and T23N, respectively). The enzyme-linked immunosorbent assay (ELISA) was also used to verify the effect of Rab10 activity on the recycling of HA-tagged M4. Only Rab10 Q68L expression reduced the cell surface level of M4 by 71%; after CCh stimulation and washout procedure, no significant differences were observed between vehicle and Rab10 WT or T23N co-expressing cells (Fig. 1e). Moreover, the internalized M4 receptors return back to the PM in 85.03% of vehicle cells and 83.06% of mCherry-Rab10 low-expressing cells, while the overexpression of mCherry-Rab10 caused cytoplasmic retention of M4 in 87.39% cells (Fig S2b, d). The effect of endogenous Rab10 alteration on the recycling of M4 was also examined. shRNA-mediated depletion of AS160, an established GAP of Rab10 [40], also caused prominent retention of M4 in 83.54% cells (Fig S2c, d and f), as observed for Rab10Q68L-expressing cells. In contrast, in shRNA-mediated Rab10-depleted cells, M4 returned to the PM normally in 84.94% cells (Fig S2c–e), as

observed for Rab10T23N-expressing cells. Collectively, the recycling of CCh-activated and internalized M4 receptors is impeded in cells with over-activated Rab10.

As a control, we further investigated the impact of Rab10-GTP on the recycling of classical clathrin-endocytic cargo protein transferrin receptor (TfR) by performing a pulse chase assay with Alexa568-labeled Tf (A568-Tf). After a 30 min pulse and chase for various periods in warm complete medium, Rab10 Q68L- and T23N-expressing cells revealed comparable uptake and recycling kinetics of Tf as with control cells (Fig. S3), indicating that GTP-locked Rab10 does not generally block the recycling of endocytic proteins due to the defect of GTPase cycle. In addition, we also determined the impact of Rab10 Q68L expression on the recycling of $G_{q/11}$ proteins-coupled M1, M3, and M5 mAChRs. As can be observed, these receptors internalize and recycle normally in the presence of Rab10 Q68L (Fig. S4a–d). Therefore, the impact of Rab10 on M4 receptor recycling might be specific.

Rab10 regulates the post-activation trafficking of M4 from EEs to REs

Next, we sought to dissect the compartment in which the endocytosed EGFP-M4 molecules were sequestered by the Rab10 Q68L expression. The EE is the sorting hub for internalized cargo proteins, where Rab5 regulates clathrin-mediated endocytosis from the PM to early/sorting endosome pools, Rab4 participates in a fast recycling pathway from the EEs to the PM, and Rab11 regulates a slow recycling pathway through the REs [41]. Using mCherry-tagged Rab5 to label EEs and Rab11 to label REs, we examined the subcellular localization of M4 receptors after CCh-induced internalization and subsequent washout processes (Fig. 1f, g). Most of the EGFP-M4 in vehicle cells is located at the PM, with minimal fluorescence signal in the cytoplasm. Line scan analysis revealed no colocalization between M4 and Rab5- or Rab11-positive endosomes (Fig. 1f, g; right). Whereas, in the cells expressing Rab10 Q68L, EGFP-M4 puncta were in the cytoplasm and prominently located at Rab5-labeled EEs, with no EGFP-M4 signals visible along the cell's perimeter (Fig. 1f). Line scan analysis showed significant colocalizaton between M4 and Rab5 fluorescent signals, but not with Rab11 (Fig. 1f, g; right). A quantitative analysis indicated that the majority of M4 puncta (58.64%) are in EEs and only 32.58% in REs (Fig. 1h). Together, these results revealed that Rab10 is involved in the transport of M4 receptors from Rab5-EEs to the Rab11-REs. Interestingly, the GTP-locked mutant Rab10, instead of the GDP-locked form, hampered the M4 recycling back to the PM, indicating that the inactivation of the Rab10 GTPase cycle is necessary for the trafficking of the activated M4 receptor through EEs.

A short sequence near the C-terminal end of ICL3 controls the M4 receptor binding to Rab10 and endosomal sorting

To understand better the molecular mechanism by which Rab10 controls the post-endocytic recycling of M4, we next evaluated whether M4 receptor was capable of forming an association with Rab10. Co-immunoprecipitation (Co-IP) experiments showed that Rab10 co-precipitated with M4 upon CCh stimulation 60 min (Fig. 2a). Moreover, only the WT and active form of Rab10 can be pulled down by M4 (Fig. 2b), demonstrating that CCh-activated M4 receptors associate with active Rab10.

We then wonder the specific motifs through which the M4 receptor interacts with Rab10. A previous study identified that the sequence ^{373}VARKFASIARNQVRKKRQMAA^{393} (V^{373}-A^{393}) in ICL3 is indispensable for M4 recycling [42]. Employing microscopy imaging, we visualized and evaluated the endocytosis of M4 ΔV^{373}-A^{393} upon CCh stimulation to be reduced by 74.76% relative to the WT receptor (Fig. S5a–c). Further, deletion of the N-terminal half ^{373}VARKFASIARNQV^{385} (V^{373}-V^{385}) did not obviously alter the extent of both endocytosis and recycling of the mutant receptor (Fig. S5a–d). Contrarily, deletion of the C-terminal half ^{386}RKKRQMAA^{393} (R^{386}-A^{393}) impaired the receptor endocytosis by 32.54% but unaltered the recycling efficiency after the removal of CCh (Fig. S5a–d). We further examined the fundamental endocytic and recycling profiles for these individual mutants (Table 1) [43, 44]. As seen, ΔR^{386}-A^{393} mutant changed the Arf6 dependence of the receptor recycling (Table 1 and Fig. S5e), as discussed later. We then compared the recycling kinetics for M4 ΔR^{386}-A^{393} and WT receptor. Surprisingly, although both receptors showed comparable recycling efficiency 60 min after removal of CCh, the M4 ΔR^{386}-A^{393} mutant returned more rapidly than the WT receptor at earlier time after removal of the agonist (Fig. S5f, g).

We were curious to address whether missing of the sequence R^{386}-A^{393} causes the M4 receptor into different endosomal sorting pathways. To this end, we tracked the localizations of internalized M4 ΔR^{386}-A^{393} to fluorescently labeled Rab-positive endosomes. According to previous studies, Rab4-positive endosome provides a fast recycling pathway, by which some endocytosed materials directly return to the PM, in contrast to through Rab11-labeled slow recycling pathway [41]. As shown, after a brief CCh stimulation for 10 min, internalized M4 ΔR^{386}-A^{393} obviously moved into Rab4-positive vesicles (Fig. 2c–f; 62.94% for M4 ΔR^{386}-A^{393} vs. 30.07% for M4 WT overlap with Rab4). More than that, even upon prolonged CCh stimulation for 60 min, M4 ΔR^{386}-A^{393} was prominently in the Rab4-labeled endosomes with few receptors traffic to Rab11-positive REs

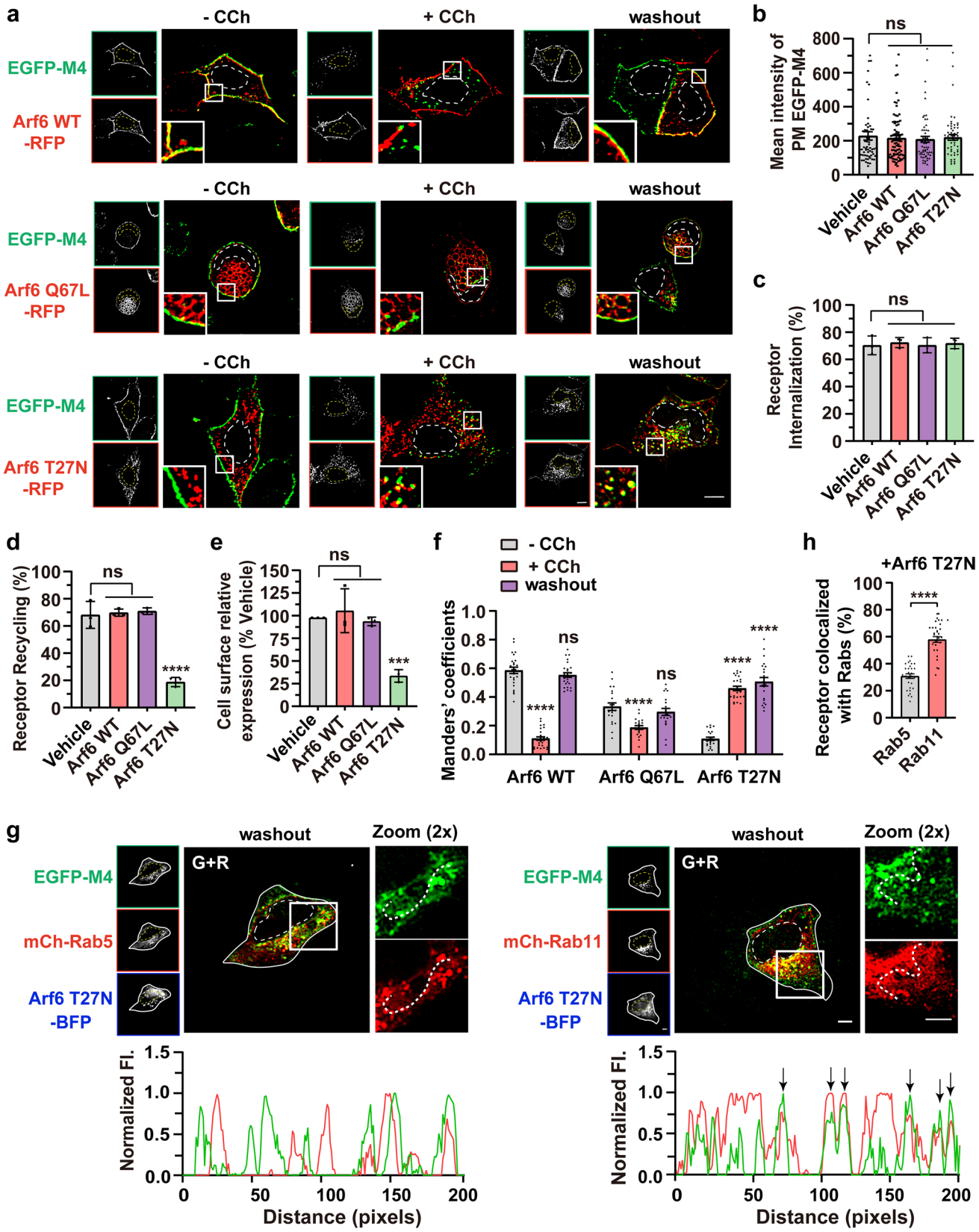
a
- CCh
+ CCh
washout
EGFP-M4
Arf6 WT -RFP
Arf6 Q67L -RFP
Arf6 T27N -RFP
b
Mean intensity of PM EGFP-M4
ns
Vehicle
Arf6 WT
Arf6 Q67L
Arf6 T27N
c
Receptor Internalization (%)
d
Receptor Recycling (%)
****
e
Cell surface relative expression (% Vehicle)
***
f
Manders' coefficients
Arf6 WT
Arf6 Q67L
Arf6 T27N
h
+Arf6 T27N
Receptor colocalized with Rabs (%)
Rab5
Rab11
g
G+R
Zoom (2x)
mCh-Rab5
mCh-Rab11
Arf6 T27N -BFP
Normalized Fl.
Distance (pixels)

◂**Fig. 3** CCh-activated and internalized EGFP-M4 is mainly hindered in the Rab11-REs in Arf6 T27N-expressing cells. **a** Representative confocal micrographs showing the subcellular localization of EGFP-M4 before or after CCh stimulation and after removal of CCh in cells expressing wild type, Q67L, or T27N Arf6-RFP. Transfected cells were untreated (left) or treated (middle) with CCh for 15 min or pretreated with CCh for 60 min followed by 60 min washout (right). Insets show the magnified boxed regions. Scale bar, 10 μm. **b–d** Quantification of the surface expression level (**b**), internalization (**c**) and recycling efficiency (**d**) of M4 receptor as measured by images shown in (**a**). Data are displayed as mean ± SEM, $n \geq 30$ cells from three independent experiments, Kruskal–Wallis test with Dunn's post hoc test in (**b**). Data represent mean ± SD from three independent experiments, one-way ANOVA followed by Dunn's post hoc test in (**c** and **d**). *ns* not significant; ****$p < 0.0001$. **e** Quantification of the recycling efficiency of HA-tagged M4 receptors using ELISA. HEK293 cells co-expressing Arf6 variants or empty vector were treated with CCh and followed by washout procedure. Data are presented as the percentage of the cell surface M4 expression level compared with vehicle group and shown as mean ± SD from 3 independent experiments. One-way ANOVA followed by Dunn's post hoc test, *ns* not significant; ***$p < 0.001$. **f** Manders' coefficients for fraction of EGFP-M4 overlapping Arf6-RFP variants as depicted in (**a**) were calculated. Data are displayed as mean ± SEM, $n \geq 20$ cells from three independent experiments, Kruskal–Wallis test with Dunn's post hoc test. *ns* not significant; ****$p < 0.0001$. **g** Representative confocal micrographs showing the overlap of internalized M4 with mCh-Rab5 (left) or mCh-Rab11 (right) after removal of CCh in Arf6 T27N co-expressing cells. Fluorescence intensity profiles are shown for the indicated region and path. Scale bar, 5 μm. **h** Colocalization of M4 receptors with Rab5 or Rab11 in Arf6 T27N-expressing cells as depicted in (**g**) was calculated. Data are displayed as mean ± SEM. $n \geq 30$ cells from three independent experiments. Unpaired two-tailed Student's *t* test. ****$p < 0.0001$. Nuclear boundaries are demarcated with dashed lines. Cell boundaries in (**g**) are demarcated with solid lines

(Fig. 2c–f; 64.52% overlap with Rab4 *vs.* 29.26% overlap with Rab11), and from where returned to the PM upon removal of the agonist (Fig. S5f and Fig. 2g). Conversely, the CCh-activated M4 WT receptor returned to the PM mainly from Rab11-labeled REs (Fig. 2c–g and Fig. S5f; 60.39% overlap with Rab11 *vs.* 37.40% overlap with Rab4 after CCh stimulation of 60 min). Taken together, although the missing of the motif R^{386}-A^{393} does not alter the PM destination of M4 receptors, it causes an itinerary switch for the internalized receptors from the slow to the fast recycling pathway (Fig. 2g).

Furthermore, we examined the impact of Rab10-GTP on the recycling of M4 ΔR^{386}-A^{393}. Cells co-expressing mCherry-Rab10 Q68L and EGFP-M4 ΔR^{386}-A^{393} were performed CCh stimulation followed by washout treatment. Unexpectedly, in contrast to the WT receptor's arrest in the cytoplasm, the M4 ΔR^{386}-A^{393} mutant receptor returned to the PM, demonstrating that missing the R^{386}-A^{393} sequence leads to the receptor transport bypassing the control by Rab10 (Fig. 2h). In addition, CCh-activated and internalized M4 receptor is colocalized with WT or Q68L Rab10 at a ratio of 45.56% or 48.07%, respectively, whereas it is colocalized with the T23N mutant only at a low level of 23.20% (Fig. S6a, b). By contrast, the internalized M4 ΔR^{386}-A^{393} mutant receptors do not colocalize with Rab10 Q68L (Fig. S6c, d). Co-IP experiment further demonstrated that, in contrast to the full-length M4 receptor, R^{386}-A^{393} deletion eliminated the precipitated Rab10 (Fig. 2a). Overall, these findings imply that the motif R^{386}-A^{393} is indispensable for the M4 receptor binding to Rab10, which confers Rab10 to regulate the M4 receptor transit from EEs to REs as a molecular brake. Disruption of this binding causes M4 recycling via the fast recycling pathway.

M4 mAChR recycles via Arf6-associated REs

ADP-ribosylation factor 6 (Arf6) is functionally associated with a subset of the so-called "clathrin/caveolin-independent" endocytic routes, where it regulates trafficking of selective cell surface integral proteins including several GPCRs [43, 45, 46]. However, the Arf6 recycling pathway seems to be dependent on the cell type, the endocytic pathway and the nature of the cargo [44]. Its involvement in the recycling of activated GPCRs still remains elusive.

We wonder how Arf6 is involved in the internalization and recycling process of agonist-activated M4. To this end, constitutively active Arf6 mutant Q67L and dominant negative mutant T27N were introduced. Previous studies revealed that the expression of the Q67L mutant hampers the Arf6 vesicles' transport and fusion with EEs, whereas the T27N mutant hinders Arf6-dependent recycling [47–50]. As anticipated, RFP-tagged Arf6 WT was primarily localized at the PM; grape-like clusters of vacuoles, characteristic of a blockade in sorting of Arf6-cargo on the way to EEs, were noticed in Arf6 Q67L-expressing cells; Arf6 T27N, however, principally appeared as punctate structures in the cytosol (Fig. 3a, left; red) [49]. None of the Arf6 variants expression affects the surface level of EGFP-M4 and extent of CCh-stimulated internalization (Fig. 3a–c). Moreover, in Arf6 Q67L-expressing cells, the internalized M4 receptors did not obviously reside in the Arf6 Q67L vacuoles (Fig. 3a, middle), further suggesting that Arf6 is not essential for M4 internalization. Interestingly, in contrast to the Arf6 WT and Q67L mutant, Arf6 T27N expression severely blocked the recycling of M4 by 72.43% (Fig. 3a, d). Quantification of the cell surface receptor using ELISA further demonstrated that the recycling of M4 was dramatically reduced by 65.73% in Arf6 T27N-expressing cells (Fig. 3e). The overlap of PM-localized M4 receptor with Arf6 WT or Q67L was comparable after recycling with respect to before internalization (Manders' coefficients: 0.55 vs. 0.59 for washout vs before CCh administration in Arf6 WT-expressing cells, and 0.30 vs. 0.33 in Arf6 Q67L-expressing cells) (Fig. 3a, f).

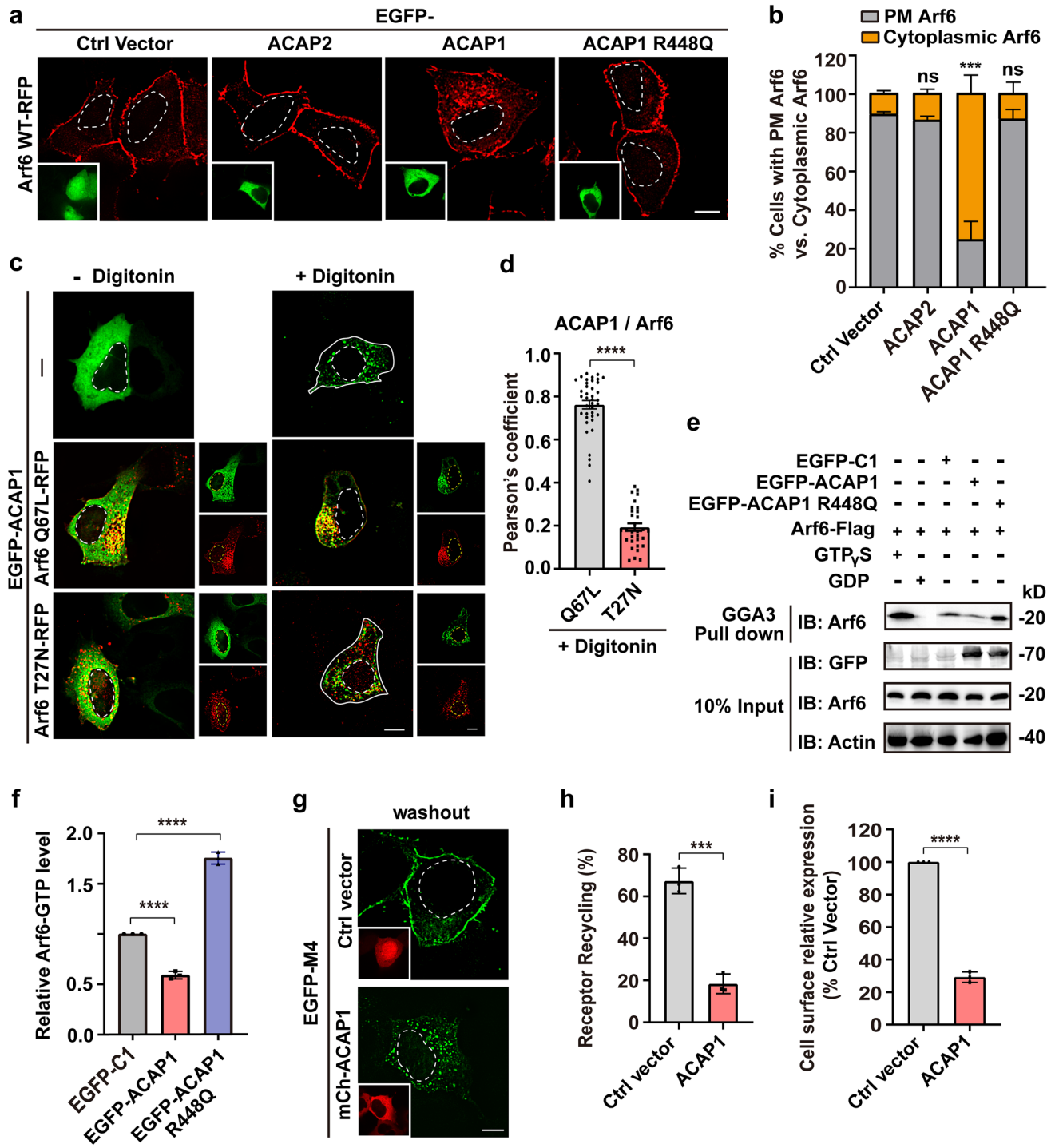

Noticeably, the cytoplasmic arrested EGFP-M4 puncta not only colocalized well with the Arf6 T27N with Manders' coefficient of 0.51 in contrast to 0.11 before CCh administration (Fig. 3a, f), but also showed prominent localization on Rab11-positive REs (57.91%) and much less position on Rab5-positive EEs (30.80%) (Fig. 3g, h). Together, these data suggest that the agonist-activated and internalized M4 in HEK293 cells returns to the PM via the Arf6-associated and Rab11-positive REs. However, the recycling of M1, M3, and M5 mAChRs was not affected by the Arf6 T27N expression (Fig. S4e, f).

◂**Fig. 4** ACAP1 is the Arf6 GAP and negatively regulates M4 recycling. **a** Representative confocal images showing the prominent translocation of Arf6-RFP from the PM to the cytoplasm in cells expressing EGFP-ACAP1, but not in cells expressing EGFP-ACAP2, ACAP1 R448Q or empty vector. Scale bar, 10 μm. **b** Quantification of the percentage of cells with PM Arf6 or cytoplasmic Arf6 in each condition shown in (**a**). Data are displayed as mean ± SD. $n = 3$ independent experiments (≥ 40 cells). Unpaired two-tailed Student's *t* test. *ns* not significant; ***$p < 0.001$. **c** Confocal images showing the subcellular distribution of EGFP-ACAP1 relative to Arf6 Q67L-RFP or Arf6 T27N-RFP. Transfected cells were untreated or treated with 50 μg/ml digitonin for 5 min at RT before image taken. Scale bar, 10 μm. **d** Quantification of the Pearson's correlation coefficients for ACAP1 with Arf6 Q67L or Arf6 T27N after digitonin treatment as depicted in (**c**). Data are displayed as mean ± SEM, $n \geq 30$ cells from three independent experiments. Unpaired two-tailed Student's *t*-test. ****$p < 0.0001$. **e** and **f** ACAP1 promotes Arf6 inactivation in HEK293 cells. **e** Cells were co-transfected with Arf6-Flag and EGFP-tagged ACAP1, ACAP1 R448Q, or empty vector. The transfected cells were lysed to analyze the protein level of activated Arf6 (Arf6-GTP) using the GST-GGA3 PBD assay. The cells only transfected with Arf6-Flag and lysed in the presence of 200 μM GTPγS or 1 mM GDP was used as positive or negative control, respectively. Elutes were analyzed by SDS-PAGE followed by immunoblotting with anti-Arf6 antibody. **f** Three independent experiments of the pulled-down Arf6-GTP level shown in (**e**) were analyzed for the gray value of protein bands. Data are displayed as mean ± SD. One-way ANOVA followed by Dunnett's post hoc test. ****$p < 0.0001$. **g** Confocal micrographs showing the recycling of EGFP-M4 after removal of CCh is impaired in cells expressing mCh-ACAP1. Scale bar, 10 μm. **h** Quantification of the recycling efficiency of EGFP-M4 in each group indicated in (**g**). Data are displayed as mean ± SD. $n = 3$ independent experiments. Unpaired two-tailed Student's *t* test. ***$p < 0.001$. **i** Quantification of the recycling efficiency of HA-tagged M4 receptors using ELISA. HEK293 cells co-expressing ACAP1 or empty vector were treated with CCh and followed by washout procedure. Data are presented as the percentage of the cell surface M4 expression level compared with vehicle group and shown as mean ± SD from 3 independent experiments. Unpaired two-tailed Student's *t* test. ****$p < 0.0001$. Nuclear boundaries are demarcated with dashed lines. Cell boundaries in (**c**) are demarcated with solid lines

ACAP1 is Arf6-GAP and negatively regulates the recycling of M4 receptors

The aforementioned results imply that small GTPases Rab10 and Arf6 are involved in the recycling of M4. These findings are reminiscent of recent discoveries that crosstalk between Rab and Rab/Arf small GTPases modulates membrane transport [31, 51–54]. We sought to address whether Rab10 and Arf6 form a cascade in regulating the post-endocytic trafficking of M4.

To test this hypothesis, first, we assessed the possibility of Arf6 GAP as a bridge between them. ACAP1 and ACAP2 are two recognized Arf6 GAP in mammalian cells [55]. Co-expressing EGFP-ACAP2 did not affect the Arf6-RFP's PM localization, as with control cells co-expressing the EGFP-C1 vector (Fig. 4a, b). Whilst, in cells expressing EGFP-ACAP1, there were a large number of punctate Arf6-RFP structures in the cytoplasm accompanied with reduced signals on the PM, representing increased inactive form of Arf6 (Fig. 4a, b). R448Q mutation has been established to inactivate the GAP function of ACAP1 [55]. As anticipated, the co-expression of ACAP1 R448Q did not affect the PM localization of Arf6 (Fig. 4a, b). Indeed, more than 76% of ACAP1-expressing cells were featured by cytoplasmic Arf6-RFP fluorescence, while only no more than 14% control and ACAP1 R448Q or ACAP2-expressing cells had cytoplasmic Arf6 signal (Fig. 4b). These results indicate that ACAP1, but not ACAP2, has the potential to inactivate Arf6 in HEK293 cells.

Next, we assessed the colocalization of ACAP1 and Arf6 Q67L, according to the fact that binding to GTP-bound GTPase will lead to the transfer of GAP from cytoplasm to endosomal membranes. ACAP1-trasfected cells were permeabilized with digitonin for 5 min to eliminate the cytosolic pool of EGFP-ACAP1 [56]. As seen, the membranous ACAP1 was exclusively positioned on the grape-like Arf6 Q67L-positive clusters of vacuoles, whereas very few were positioned on the Arf6 T27N vesicles (with Pearson's coefficient of 0.76 vs 0.19 for ACAP1 with Arf6 Q67L vs T27N) (Fig. 4c, d). These results demonstrate that ACAP1 indeed promotes the transition of Arf6 from an active state to an inactive state in HEK293 cells.

The amounts of active Arf6 are controlled in part by its GAP. Employing the Arf6 effector GGA3 (Golgi-associated, gamma adaptin ear-containing, Arf-binding protein 3), an effector-binding assay was performed to analyze the level of active Arf6 affected by the expression of ACAP1 (Fig. 4e) [57]. The protein-3 binding domain (PBD) of GGA3 fused to glutathione S-transferase (GST) (GST-GGA3-PBD) was incubated with lysates from the cells co-transfected with Arf6-Flag and EGFP-ACAP1 or R448Q mutant. Quantification of the Arf6 activity revealed that co-expressing ACAP1 reduced the level of Arf6-GTP to 59.13% of control cells, whereas the GAP mutant R448Q led to an increase of about 1.75-fold in the level of Arf6-GTP (Fig. 4f), further supporting that ACAP1 is the Arf6 GAP in HEK 293 cells. Consequently, in ACAP1-expressing cells, the recycling efficiency of M4 receptor was reduced from 67.36 to 18.33% (Fig. 4g, h), as with Arf6 T27N cells (Fig. 3a, d). ELISA assay also revealed that the cell surface recycling of M4 receptors was heavily decreased by 70.85% in ACAP1-expressing cells (Fig. 4i). Together, the Arf6-GAP ACAP1 negatively regulates the recycling of M4 receptor.

Rab10-GTP binds and recruits ACAP1 onto endosomes

We then examined whether Rab10 binds to ACAP1. Co-IP experiments were performed using HEK293 cells co-transfected with HA-ACAP1 and 3xFlag-tagged Rab10 WT, Q68L, or T23N mutant. Rab10 proteins were purified from HEK293

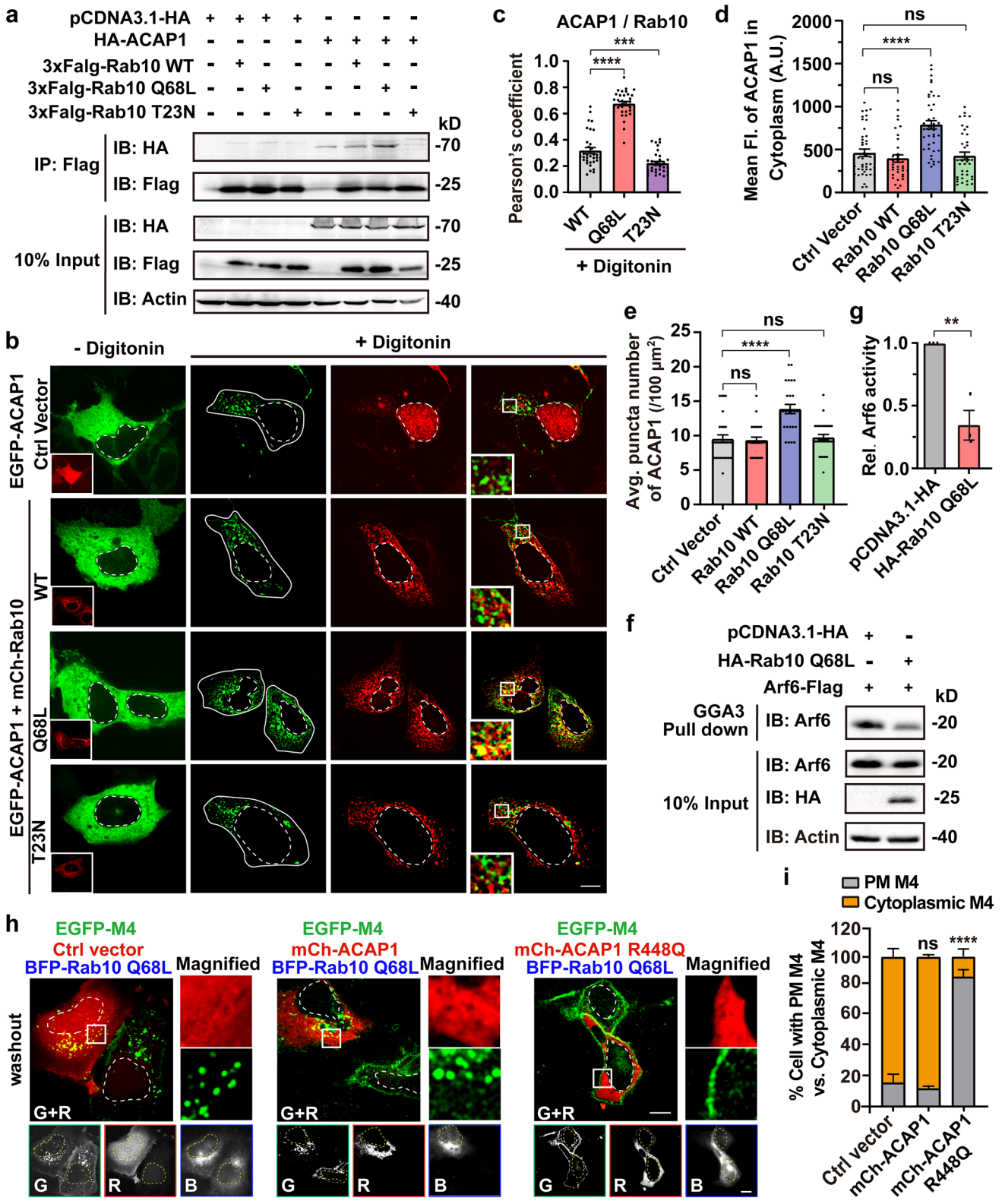

cell lysates using Flag-beads, and ACAP1 was detected together with Rab10 WT or its active mutant Q68L, but not the inactive mutant T23N, indicating that ACAP1 binds to Rab10 and prefers the active form of Rab10 (Fig. 5a). To further examine whether ACAP1 is recruited to endosomes by Rab10-GTP, we investigated the effect of Rab10 variants expression on the level of membrane-bound ACAP1, based on the fact that the subcellular localization of GAP switches between

◂**Fig. 5** The GAP activity of ACAP1 is indispensable for Rab10-GTP resultant Arf6 inactivation and defective M4 recycling. **a** ACAP1-Rab10 interaction was assessed in lysates of HEK293 cells transiently expressing HA-ACAP1 and 3 × Flag-tagged Rab10 WT, Q68L, or T23N mutant, respectively. Lysates were IP through the HA epitope followed by immunoblotting using anti-Flag and anti-HA antibodies. **b** Confocal images showing the subcellular distribution of ACAP1 in indicated context. Transfected cells were untreated or treated with 50 μg/ml digitonin for 5 min at RT before image taken. Insets show the expression of mCh-Rab10 variants (− Digitonin) or the magnified boxed regions (+Digitonin). Scale bar, 10 μm. **c** Quantification of the Pearson's correlation coefficients for ACAP1 with Rab10 variants after digitonin treatment as depicted in (**b**). Data are displayed as mean ± SEM, $n \geq 30$ cells from three independent experiments, Kruskal–Wallis test with Dunn's post hoc test. ***$p < 0.001$; ****$p < 0.0001$. **d** and **e** Quantification of the average Fluorescence intensity (**d**) and puncta number (**e**) of ACAP1 in digitonin-treated cells as (**b**) indicates. Data are displayed as mean ± SEM. $n \geq 30$ cells from three independent experiments. Kruskal–Wallis test with Dunn's post hoc test. *ns* not significant; ****$p < 0.0001$. **f** Expressing Rab10 Q68L reduces the Arf6-GTP amount in HEK293 cells. Cells were co-transfected with Arf6-Flag and HA-Rab10 Q68L or control empty vector. The protein level of activated Arf6 (Arf6-GTP) was assessed using the GST-GGA3 PBD assay. Elutes were analyzed by SDS-PAGE followed by immunoblotting with anti-Arf6 antibody. **g** Three independent experiments of the pulled-down Arf6-GTP level shown in (**f**) were analyzed for the gray value of protein bands. Data are displayed as mean ± SD. Unpaired two-tailed Student's *t* test. **$p < 0.01$. **h** Rab10 Q68L resultant defective M4 recycling is reversed by co-expressing ACAP1 R448Q. HEK293 cells were co-transfected with EGFP-M4, BFP-Rab10 Q68L, and mCherry-tagged ACAP1, ACAP1 R448Q, or control empty vector. Boxed areas are magnified into separate channels on the right. G/R/B represents the green/red/blue channel, respectively. Scale bar, 10 μm. **i** Quantification of the percentage of cells with PM M4 or cytoplasmic M4 in each condition shown in (**h**). Data are displayed as mean ± SD. $n = 3$ independent experiments (≥ 30 cells). Unpaired two-tailed Student's *t*-test. *ns* not significant; ****$p < 0.0001$. Nuclear boundaries are demarcated with dashed lines. Cell boundaries in (**b**) are demarcated with solid lines

the cytosol and the endomembrane according to its activity. Membrane fractionation assay indicated that co-expressing Rab10 Q68L produced an enhanced level of membrane-associated ACAP1 (2.38-fold vs. control), whereas Rab10 T23N resulted in a mild reduction in membrane-associated ACAP1 (75.31% vs. control) (Fig. S7a, b). Confocal microscopy was also performed to evaluate the impact of Rab10 variants on the endomembrane association of EGFP-ACAP1. Although ACAP1 is evenly distributed predominately throughout the cytoplasm (- digitonin), the punctate fluorescence signals are visible after digitonin treatment and correspond to endosomal membrane-associated EGFP-ACAP1 (Fig. 5b). Notably, the vesicular ACAP1 depicted strong colocalization with Rab10 Q68L (Fig. 5b, c; with Pearson's coefficient of 0.68 vs 0.32 or 0.22 for ACAP1 with Rab10 Q68L vs WT or T23N), which are also positive for EEA1 staining (Fig. S7c). Furthermore, the fluorescence intensity (FI) and puncta number of vesicular EGFP-ACAP1 increased in cells co-expressing Rab10 Q68L than that in control cells (Fig. 5d, e), demonstrating that Rab10-GTP facilitates the recruitment of ACAP1 to the sorting endosome.

Rab10 negatively regulates Arf6 activity via ACAP1 to impair M4 recycling

Next, we sought to address whether Rab10 and Arf6 form a cascade mediated by ACAP1. To this end, the GGA3 effector-binding assay was carried out to examine whether Rab10-GTP expression reduce the level of active Arf6 (Fig. 5f, g). The active Arf6 pulled down by GGA3 in Rab10 Q68L expressing cells is 35.2% of the control level, supporting that elevated Rab10-GTP expression recruits ACAP1 and reduces Arf6-GTP levels. Further, we examined the effect of ACAP1 activity on Rab10-GTP-impaired M4 recycling. Co-expressing mCherry-ACAP1 with BFP-Rab10 Q68L caused cytoplasmic retention of EGFP-M4 in 86.34% cells. In contrast, EGFP-M4 returns to the PM normally in 85.6% Rab10 Q68L and ACAP1 R448Q co-expressing cells (Fig. 5h, i). These findings indicated that besides binding to M4 receptors, Rab10-GTP also creates an environment that favors ACAP1-mediated Arf6 inactivation, thereafter causes blockage of M4 recycling. However, the R448Q mutant of Arf6-GAP ACAP1 reverses the Rab10-GTP resultant defective recycling of M4. Overall, these results indicate that ACAP1 bridges the Rab10/Arf6 GTPases cascade, which regulates the recycling of the agonist-activated M4 receptor.

Rab10/Arf6-mediated recycling is critical for the resensitization of M4 receptors

mAChRs undergo desensitization and rapid internalization on ligand exposure and subsequently recycle back to the cell surface in one hour [22, 33]. Once recycled to the PM, many receptors resensitize, i.e., functionally recover, such that their responsiveness toward the agonist is restored. Next, we explored the function(s) of Rab10 and Arf6 in M4-mediated signaling. M4 receptor couples to the G_i/G_o family G proteins, and its activation has been well demonstrated to inhibit adenylyl cyclases, stimulate phospholipase C, and induce receptor-mediated elevation of $[Ca^{2+}]_i$, which is pertussis toxin (PTX)-sensitive [38, 58].

We chose the $[Ca^{2+}]_i$ elevation as a functional readout and assessed the original Ca^{2+} signal and the resensitizing signal using Fluo-4 AM Ca^{2+} fluorescence probe. CHO-K1 cells expressing RFP-M4 were seeded in a 1:1 ratio with plain cells and co-cultured 24 h before Ca^{2+} assay. As pictured by the experimental paradigm (Fig. 6a), the original Ca^{2+} flux is mediated by the initial surface M4 receptors, while the resensitizing Ca^{2+} signal will be elicited by regenerated PM M4 deriving from internalization and subsequent recycling. The benefit of this image-based Ca^{2+} flux assay is that the

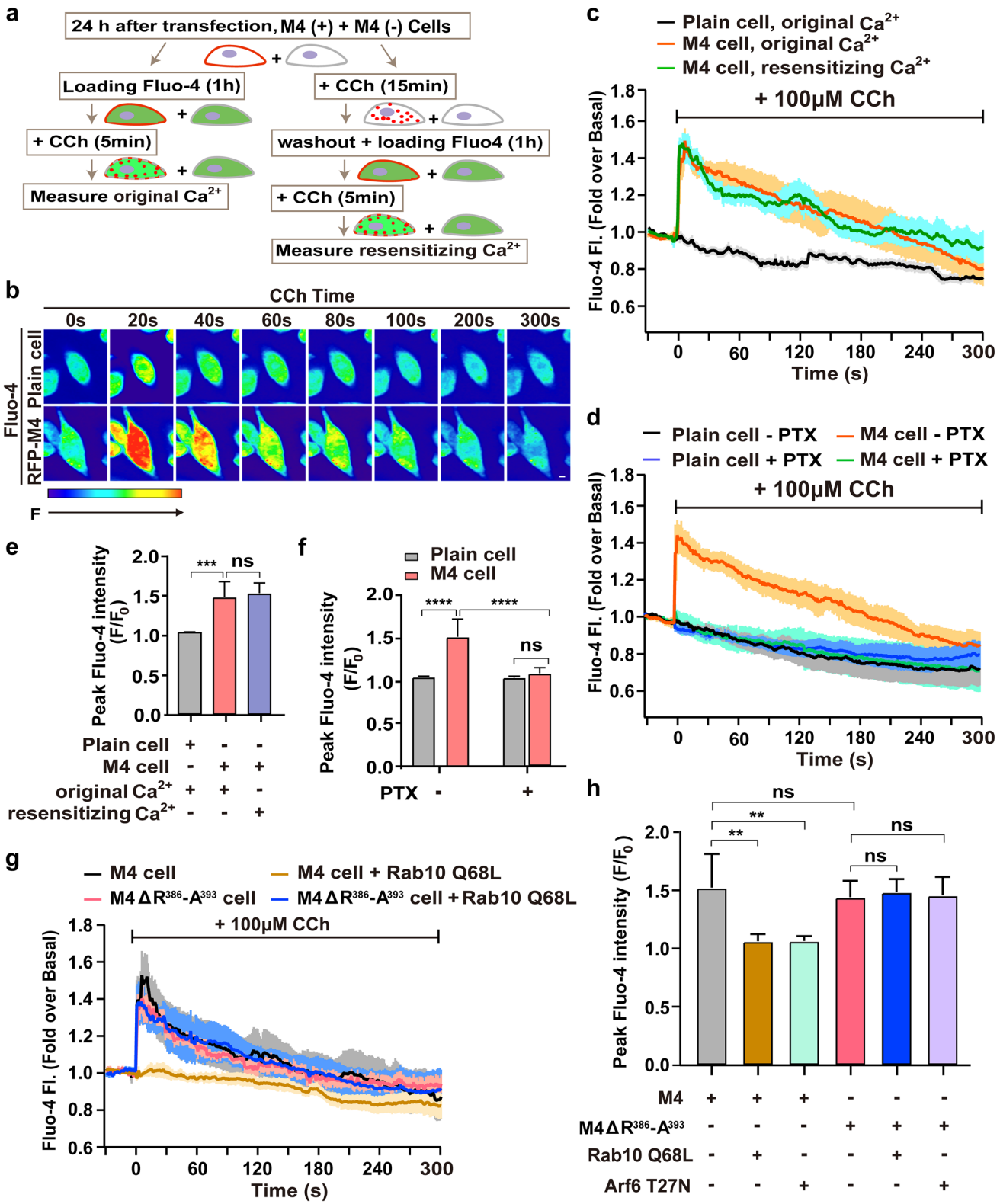
a
24 h after transfection, M4 (+) + M4 (-) Cells
Loading Fluo-4 (1h)
+ CCh (5min)
Measure original Ca2+
+ CCh (15min)
washout + loading Fluo4 (1h)
+ CCh (5min)
Measure resensitizing Ca2+
b
CCh Time
0s 20s 40s 60s 80s 100s 200s 300s
Fluo-4
Plain cell
RFP-M4
F
c
Plain cell, original Ca2+
M4 cell, original Ca2+
M4 cell, resensitizing Ca2+
+ 100μM CCh
Fluo-4 Fl. (Fold over Basal)
Time (s)
d
Plain cell - PTX
M4 cell - PTX
Plain cell + PTX
M4 cell + PTX
+ 100μM CCh
Fluo-4 Fl. (Fold over Basal)
Time (s)
e
Peak Fluo-4 intensity (F/F0)
*** ns
Plain cell
M4 cell
original Ca2+
resensitizing Ca2+
f
Plain cell
M4 cell
Peak Fluo-4 intensity (F/F0)
**** ****
ns
PTX
g
M4 cell
M4 cell + Rab10 Q68L
M4ΔR386-A393 cell
M4ΔR386-A393 cell + Rab10 Q68L
+ 100μM CCh
Fluo-4 Fl. (Fold over Basal)
Time (s)
h
Peak Fluo-4 intensity (F/F0)
ns
**
**
ns
ns
M4
M4ΔR386-A393
Rab10 Q68L
Arf6 T27N

◂**Fig. 6** Disruption of Rab10/Arf6 cascade affects M4-mediated Ca^{2+} signal resensitization. **a** Schematic diagram illustrates Fluo-4-based intracellular calcium assay. **b** Color-coded fluorescence intensity changes show the dynamics of intracellular Ca^{2+} in response to CCh application in CHO-K1 cells expressing RFP-M4 (lower) or not (upper). Red indicates a large increase in Ca^{2+}; blue indicates little increase in Ca^{2+}. Scale bar, 10 μm. **c** Average normalized curves for Fluo-4 fluorescence intensity change upon CCh stimulation in cells expressing RFP-M4 or not. The original or resensitizing Ca^{2+} signal was induced by CCh administration as denoted in (**a**). **d** Effect of PTX treatment on the CCh-induced Fluo-4 fluorescence intensity change in M4-expressing cells. Co-cultured RFP-M4-expressing and plain cells were left untreated (- PTX) or pre-treated with 100 ng/ml PTX for 12 h (+PTX) and administrated with CCh to activate M4. **e** and **f** Analysis of the fold increase of peak intracellular Ca^{2+} as depicted in (**c**) and (**d**), respectively. Data represent the mean ± SD of at least five independent experiments. One-way ANOVA followed by Tukey's post hoc test (**c**). Two-way ANOVA followed by Tukey's post hoc test (**d**). *ns* not significant; ***$p < 0.001$; ****$p < 0.0001$. **g** The effect of Rab10 Q68L on the resensitizing Ca^{2+} signal in M4 WT and ΔR^{386}-A^{393} mutant-expressing cells. Resensitizing Ca^{2+} flux was initiated by repeated CCh treatment and examined as illustrated in diagram (**a**). **h** Histograms showing the fold increase of peak intracellular Ca^{2+} in each indicated condition. Data represent the mean ± SD of at least five independent experiments. One-way ANOVA followed by Tukey's post hoc test. *ns* not significant; **$p < 0.01$

Ca^{2+} signals for the M4-expressing cells and the blank cells will be obtained simultaneously and exactly under the same context. The red fluorescence channel was utilized to identify RFP-M4 positive-expressing or neighboring negative-expressing cells, while the green fluorescence channel was utilized to collect Fluo-4 fluorescence with 1-s intervals for 5 min.

We first examined whether CCh application elicits Ca^{2+} flux in M4-expressing cells without or with washout procedure. Figure 6b shows the representative Ca^{2+} flux changes upon CCh application in cells expressing RFP-M4 or not [59]. As seen, the untransfected cells showed no increase in Fluo-4 fluorescence upon CCh application (Fig. 6b), in line with a low level of endogenous M-type AChRs expressed in CHO-K1 cells [60]. Whereas, CCh activation led to instant Ca^{2+} elevation in the RFP-M4-positive cells (Fig. 6b). The peak fluorescence intensity triggered by CCh in the M4-positive cells was 1.48-fold to the basal level and Ca^{2+} signal finally dropped to the steady state in 300 s (Fig. 6c, d). Remarkably, repetitive CCh application on RFP-M4-positive cells after washout procedure

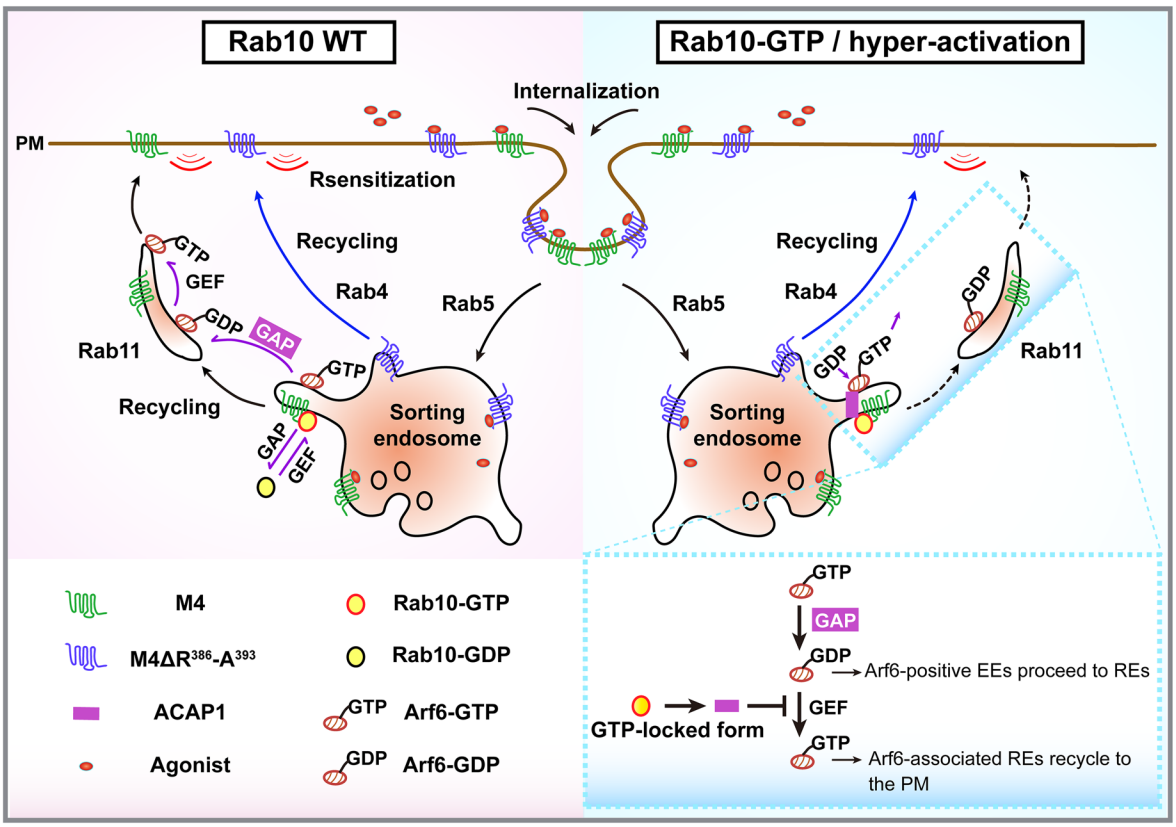

Fig. 7 A model of the GTPase cascade between Rab10 and Arf6 via ACAP1 controlling M4 mAChR transit through endosomes. Rab10 is recruited to the Arf6-positive sorting endosomes and recruits its effector, Arf6 GAP-ACAP1, to the same compartment. ACAP1 then inactivates Arf6. Agonist-activated and internalized M4 receptor binds to the GTP-Rab10, hence over activation of Rab10 leads to hampered recycling of M4 on Rab5-positive endosomes. Aberrant inactivation of Arf6, however, hinders the recycling of M4 predominantly on Rab11-positive endosomes. M4 receptor missing the R^{386}-A^{393} motif will bypass the control of Rab10 and directly returns to the PM via Rab4-positive early endosomes

indeed elicited the resensitizing Ca^{2+} signal, with similar peak amplitude and decline kinetics to the original signal (Fig. 6c, e). Next, we examined whether the CCh-activated Ca^{2+} signal is PTX-sensitive in RFP-M4-expressing cells. As shown, CCh application had no Ca^{2+} increase in the plain cells whether pretreated with PTX or not. However, pretreatment with PTX eliminated the CCh-activated original Ca^{2+} elevation in RFP-M4-expressing cells (Fig. 6d, f), supporting that M4-mediated Ca^{2+} increase is PTX sensitive. These preliminary results indicate that this experimental paradigm is appropriate to further examine the signal resensitization of M4 impacted by abnormal endosomal trafficking.

We next evaluated the effect of interfering with Rab10/Arf6 cascade on the M4 receptor-mediated Ca^{2+} signal resensitization. First, RFP-M4-expressing CHO-K1 cells were co-transfected with BFP-Rab10 Q68L. In contrast to the instant M4-mediated Ca^{2+} elevation responding to repetitive CCh stimulation, co-expressing Rab10 Q68L resulted in the elimination of Ca^{2+} signal resensitization (Fig. 6g, h), indicating that the Rab10 Q68L abolishes M4-mediated signal resensitization due to defective recycling of the functional receptor to the PM. Furthermore, M4 mutant receptor missing the R^{386}-A^{393} motif elicited a similar resensitizing Ca^{2+} signal as with the WT receptors, which was not impacted by the co-expressing Rab10 Q68L (Fig. 6g, h), validating our hypothesis that the mutant receptor recycles to the PM normally and bypasses sequestration by Rab10-GTP and implying that the mutation does not affect signal transduction. Likewise, we also verified that co-expressing Arf6 T27N abolished resensitization of the M4-mediated Ca^{2+} signal (Fig. 6h). However, removing the motif R^{386}-A^{393} will allow the mutant receptor to resensitize by escaping the control of Arf6-regulated recycling (Fig. 6h). These results strongly imply that post-endocytic trafficking eventually impacts the receptor-mediated signal resensitization.

Discussion

In this study, we identify the Rab10/Arf6 GTPase cascade as a regulator of M4 mAChR sorting and transport along the endosomal recycling pathway. Arf6 GAP-ACAP1 bridges this cascade. We illustrate that agonist-activated M4 mAChR binds to GTP-bound Rab10 and the R^{386}-A^{393} motif within ICL3 is necessary for this binding. Further, activated Rab10 arrests the internalized M4 predominantly on Rab5-positive EEs and hampers resensitization of the M4-mediated Ca^{2+} signal. Moreover, M4 mutant receptor missing the motif R^{386}-A^{393} can bypass control by the Rab10/Arf6 cascade and returns to the PM through the Rab4-positive fast recycling pathway. Therefore, Rab10 couples the cargo sorting and membrane trafficking regulation through cycle between GTP-bound and GDP-bound state, which makes it function like a molecular brake to regulate the trafficking and concomitant signaling of M4 (Fig. 7).

Rab proteins orchestrate vesicular trafficking; when GTP is bound, they recruit specific effector proteins to the membrane surfaces to mediate transport vesicle formation, motility, and target recognition. Multiple studies have reported that Rabs can also bind directly to cargo proteins. Interestingly, most of these cargo proteins are GPCR signal receptors [26]. For example, Rab43 selectively regulates the transport of nascent GPCRs from the ER to the Golgi through direct and activation-dependent interaction with the receptors on the secretory pathway [28, 61]. Likewise, Rab8 and Rab26 interact with specific GPCRs and modulate their Golgi to cell surface transport [52, 62]. Rab5 and Rab11 were demonstrated on the endocytic pathway to bind GPCR cargos directly and regulate their trafficking [5, 63]. But, less well understood is how mechanically the individual Rab proteins regulate the transport of cargo GPCRs.

Here, we revealed that Rab10 associates with M4 mAChR on one hand and regulates recycling transport via Rab10/ACAP1/Arf6 cascade on the other hand, which couples the cargo sorting to membrane transport process and enables the precise control of M4 transit through the endosomes and signal. Different from presently known Rab-GPCR couples, in which Rab activation is necessary for GPCR protein's normal transport. For example, β_2AR associates with the GDP-bound Rab11, thus siRNA knockdown of Rab11 or expression of dominant-negative Rab11 mutant interferes with receptor trafficking [5]. M4 mAChR binds the active form of Rab10, inactivation of Rab10 through GTP-to-GDP hydrolysis is essential for the M4 cargo transport to REs and PM. This is possibly due to the unique cascade of Rab10/Arf6 and concomitant negative regulation of Rab10 for the Arf6-associated recycling pathway. Notably, our and other previous studies on *C. elegans* showed that the post-endocytic trafficking of the classical clathrin-independent endocytic (CIE) cargo IL-2 receptor α-chain (TAC) is blocked by loss of Rab-10 or inactive Rab-10 T23N mutant but not by active Rab-10 Q68L [64, 65], strongly indicating that Rab10 plays different roles in mediating the post-endocytic trafficking of subgroups of CDE and CIE cargoes and that Rab10 is a versatile regulator of various trafficking itineraries on not only biosynthetic but also post-endocytic pathways [27, 32]. Further, different from most of the recognized Rab binding sites that are mainly localized within the carboxyl-terminal tails of GPCRs [66], here we find that a short sequence R^{386}-A^{393} in ICL3 of M4 receptor is essential for its association with Rab10 GTPase. Mutant receptor missing this motif is able to bypass the control of Rab10/Arf6 cascade and returns to the PM via Rab4-positive fast recycling pathway, instead of retention in endosomes or mis-trafficking to lysosomes for degradation. In all, although amounts of studies showed PDZ ligands acted as recycling sequences in

the C-terminal tails of many GPCRs, our results provide the first clue that Rab10 is able to function as scaffold protein to recognize specific recycling sequence other than PDZ ligand and control the endosome sorting of M4 AChR in a way different from its acknowledged role in recycling in polarized cells [25].

Both Rab-type and Arf-type small GTPases act as molecular switches that drive or halt membrane trafficking by cycling between a GTP-bound active state and a GDP-bound inactive state [67, 68]. Accumulating evidence has revealed that they control highly diverse membrane trafficking routes in a coordinated manner [69]. For instance, Rab11-FIP3/Arfophilin-1 mediates crosstalk between Rab11 and Arf6 to regulate membrane traffic in cytokinesis [70], and Rab35/Arf6 cascade mediated by centaurin-β2, an Arf6-GAP, is implicated in neurite outgrowth of PC12 cells [52]. Allaire et al. anticipated that Rab35 and Arf6 also form a mutually antagonistic module to coordinate cell adhesion and migration by controlling cargo recycling [54]. Shi et al. previously identified a *C. elegans* Rab-10-to-Arf6 regulatory loop required to regulate endosomal $PI(4,5)P_2$ [53]. However, till now what membrane cargo proteins are transported under control by this Rab10-to-Arf6 cascade has not yet known.

Here, we identified for the first time the cargo proteins transported though the Rab10/Arf6 cascade, which points to the possible impact on M4 signaling by disruption of this membrane trafficking process. $G_{q/11}$-coupled M1, M3, and M5 internalize via clathrin-dependent process and afterwards recycle back to the PM for reuse, whose trafficking itineraries are similar to the M4 receptor. Nonetheless, our results showed that neither constitutively active Rab10 Q68L nor dominant negative mutant Arf6 T27N affected post-activation recycling of these mAChRs. For this different effect of Rab10/Arf6 cascade in regulating various subtypes of recycling mAChRs, one possible explanation might be the interaction between Rab10 and the small linear motifs in the ILC3 of M4 is modulated by flanking residues outside the motif, which obviously needs further investigation. We did not evaluate the impact on the M2 receptor, since it is degraded in lysosomes but not recycled back to the PM [33]. Nevertheless, the distinct dependence of M4 mAChR on Rab10/Arf6 cascade indicates that the close interaction or regulation of Rab10 for M4 is specific among the mAChR family.

Abnormal GPCR trafficking and signaling are directly linked to pathogenesis of a number of neurologic disorders, for which GPCRs are direct primary therapeutic targets. Mutations for Rabs and modifications in Rab-mediated membrane trafficking are also connected to the progression of neurodegenerative diseases, including AD, Parkinson's, and Huntington's diseases [71, 72]. Hypothetically, modulating the activity of Rab10 will alter the balance of M4 receptors between the PM and endosomal residential pool. Here, we demonstrated that both elevated Rab10 WT expression level and siRNA knockdown of Rab10-GAP AS160, which produces enhanced Rab10-GTP, lead to defective M4 recycling. Actually, although M4 mAChR is an attractive drug target for the treatment of AD or schizophrenia, its trafficking feature in patients with neurologic disorders is far from clear. Future advancements in specialized antibodies to recognize different mAChR subtypes will be expected to address the implication of Rab10 in M4 mAChR trafficking in primary neurons or in vivo. In all, we reveal that Rab10 acts as a molecular brake to regulate the endosomal sorting and recycling of M4 mAChR via Rab10/Arf6 cascade. Further studies are needed to define the functional roles of Rab10-mediated M4 trafficking and sorting in the pathology of neurological diseases, as may provide intervention strategies via targeting the trafficking processes of M4 in the treatment of M4-associated neurologic diseases.

Supplementary Information The online version contains supplementary material available at https://doi.org/10.1007/s00018-023-04722-x.

Acknowledgements We thank Dr. Victor Hsu (Brigham and Women's Hospital, Department of Medicine, Harvard Medical School, Boston, MA 02115, USA), Dr. Emmanuel Boucrot (Institute of Structural and Molecular Biology, University College London, London, UK), and Dr. Eli Song(Institute of Biophysics, Chinese Academy of Sciences, Beijing, China) for kindly donating material. This work was supported by the Major Research Plan of the National Natural Science Foundation of China (91954107), and the National Natural Science Foundation of China (32270739, 31571468) to RZ.

Author contributions Conceptualization, RZ; Investigation, RX, MW, XS, SM, and LZ; Methodology, RX, PY, MW, XS, and RZ; Formal analysis, RX, and MW; Funding acquisition, RZ; Project administration, PY, RZ; Original draft, RZ; Writing and review and editing, RX, PY, MW, and RZ.

Funding This work was supported by the Major Research Plan of the National Natural Science Foundation of China (91954107), and the National Natural Science Foundation of China (32270739, 31571468) to RZ.

Availability of dada and material All plasmids and data generated in this study will be freely provided upon request to the corresponding author.

Declarations

Conflict of interest The authors declare no competing interests.

Ethical approval Not applicable.

Consent to participate Not applicable.

Consent for publish Not applicable.

References

1. Hauser AS, Attwood MM, Rask-Andersen M, Schioth HB, Gloriam DE (2017) Trends in GPCR drug discovery: new agents, targets and indications. Nat Rev Drug Discov 16:829–842. https://doi.org/10.1038/nrd.2017.178
2. Wei Z, Zhang M, Li C, Huang W, Fan Y, Guo J, Khater M, Fukuda M, Dong Z, Hu G, Wu G (2019) Specific TBC domain-containing proteins control the ER-Golgi-plasma membrane trafficking of GPCRs. Cell Rep 28:554–566. https://doi.org/10.1016/j.celrep.2019.05.033. (**e554**)
3. Sposini S, Hanyaloglu AC (2017) Spatial encryption of G protein-coupled receptor signaling in endosomes; Mechanisms and applications. Biochem Pharmacol 143:1–9. https://doi.org/10.1016/j.bcp.2017.04.028
4. Gupta MK, Mohan ML, Naga Prasad SV (2018) G Protein-coupled receptor resensitization paradigms. Int Rev Cell Mol Biol 339:63–91. https://doi.org/10.1016/bs.ircmb.2018.03.002
5. Parent A, Hamelin E, Germain P, Parent JL (2009) Rab11 regulates the recycling of the β2-adrenergic receptor through a direct interaction. Biochem J 418:163–172. https://doi.org/10.1042/BJ20080867
6. Abdullah N, Beg M, Soares D, Dittman JS, McGraw TE (2016) Downregulation of a GPCR by β-arrestin2-mediated switch from an endosomal to a TGN recycling pathway. Cell Rep 17:2966–2978. https://doi.org/10.1016/j.celrep.2016.11.050
7. Sposini S, Jean-Alphonse FG, Ayoub MA, Oqua A, West C, Lavery S, Brosens JJ, Reiter E, Hanyaloglu AC (2017) Integration of GPCR signaling and sorting from very early endosomes via opposing APPL1 mechanisms. Cell Rep 21:2855–2867. https://doi.org/10.1016/j.celrep.2017.11.023
8. Maxfield FR, McGraw TE (2004) Endocytic recycling. Nat Rev Mol Cell Biol 5:121–132. https://doi.org/10.1038/nrm1315
9. Romero G, von Zastrow M, Friedman PA (2011) Role of PDZ proteins in regulating trafficking, signaling, and function of GPCRs: means, motif, and opportunity. Adv Pharmacol 62:279–314. https://doi.org/10.1016/B978-0-12-385952-5.00003-8
10. Hanyaloglu AC, von Zastrow M (2008) Regulation of GPCRs by endocytic membrane trafficking and its potential implications. Annu Rev Pharmacol Toxicol 48:537–568. https://doi.org/10.1146/annurev.pharmtox.48.113006.094830
11. Nooh MM, Mancarella S, Bahouth SW (2018) Novel paradigms governing β1-adrenergic receptor trafficking in primary adult rat cardiac myocytes. Mol Pharmacol 94:862–875. https://doi.org/10.1124/mol.118.112045
12. Jean-Alphonse F, Bowersox S, Chen S, Beard G, Puthenveedu MA, Hanyaloglu AC (2014) Spatially restricted G protein-coupled receptor activity via divergent endocytic compartments. J Biol Chem 289:3960–3977. https://doi.org/10.1074/jbc.M113.526350
13. Paquet M, Asay MJ, Fam SR, Inuzuka H, Castleberry AM, Oller H, Smith Y, Yun CC, Traynelis SF, Hall RA (2006) The PDZ scaffold NHERF-2 interacts with mGluR5 and regulates receptor activity. J Biol Chem 281:29949–29961. https://doi.org/10.1074/jbc.M602262200
14. Temkin P, Lauffer B, Jager S, Cimermancic P, Krogan NJ, von Zastrow M (2011) SNX27 mediates retromer tubule entry and endosome-to-plasma membrane trafficking of signalling receptors. Nat Cell Biol 13:715–721. https://doi.org/10.1038/ncb2252
15. Hirakawa T, Galet C, Kishi M, Ascoli M (2003) GIPC binds to the human lutropin receptor (hLHR) through an unusual PDZ domain binding motif, and it regulates the sorting of the internalized human choriogonadotropin and the density of cell surface hLHR. J Biol Chem 278:49348–49357. https://doi.org/10.1074/jbc.M306557200
16. Marchese A, Paing MM, Temple BR, Trejo J (2008) G protein-coupled receptor sorting to endosomes and lysosomes. Ann Rev Pharmacol Toxicol 48:601–629. https://doi.org/10.1146/annurev.pharmtox.48.113006.094646
17. Zenko D, Hislop JN (2018) Regulation and trafficking of muscarinic acetylcholine receptors. Neuropharmacology 136:374–382. https://doi.org/10.1016/j.neuropharm.2017.11.017
18. van der Westhuizen ET, Choy KHC, Valant C, McKenzie-Nickson S, Bradley SJ, Tobin AB, Sexton PM, Christopoulos A (2020) Fine tuning muscarinic acetylcholine receptor signaling through allostery and bias. Front Pharmacol 11:606656. https://doi.org/10.3389/fphar.2020.606656
19. Yohn SE, Conn PJ (2018) Positive allosteric modulation of M1 and M4 muscarinic receptors as potential therapeutic treatments for schizophrenia. Neuropharmacology 136:438–448. https://doi.org/10.1016/j.neuropharm.2017.09.012
20. Foster DJ, Choi DL, Conn PJ, Rook JM (2014) Activation of M1 and M4 muscarinic receptors as potential treatments for Alzheimer's disease and schizophrenia. Neuropsychiatr Dis Treat 10:183–191. https://doi.org/10.2147/NDT.S55104
21. Vogler O, Nolte B, Voss M, Schmidt M, Jakobs KH, van Koppen CJ (1999) Regulation of muscarinic acetylcholine receptor sequestration and function by beta-arrestin. J Biol Chem 274:12333–12338. https://doi.org/10.1074/jbc.274.18.12333
22. Volpicelli LA, Lah JJ, Fang G, Goldenring JR, Levey AI (2002) Rab11a and myosin Vb regulate recycling of the M4 muscarinic acetylcholine receptor. J Neurosci 22:9776–9784
23. Bao Z, Zhou S, Zhou H (2020) Sorting Nexin 27 as a potential target in G proteincoupled receptor recycling for cancer therapy (Review). Oncol Rep 44:1779–1786. https://doi.org/10.3892/or.2020.7766
24. Stenmark H (2009) Rab GTPases as coordinators of vesicle traffic. Nat Rev Mol Cell Biol 10:513–525. https://doi.org/10.1038/nrm2728
25. Chua CEL, Tang BL (2018) Rab 10-a traffic controller in multiple cellular pathways and locations. J Cell Physiol 233:6483–6494. https://doi.org/10.1002/jcp.26503
26. Dong C, Wu G (2013) G-protein-coupled receptor interaction with small GTPases. Methods Enzymol 522:97–108. https://doi.org/10.1016/B978-0-12-407865-9.00006-6
27. Degrandmaison J, Abdallah K, Blais V, Genier S, Lalumiere MP, Bergeron F, Cahill CM, Boulter J, Lavoie CL, Parent JL, Gendron L (2020) In vivo mapping of a GPCR interactome using knockin mice. Proc Natl Acad Sci USA 117:13105–13116. https://doi.org/10.1073/pnas.1917906117
28. Wei Z, Xu X, Fang Y, Khater M, Naughton SX, Hu G, Terry AV Jr, Wu G (2021) Rab43 GTPase directs postsynaptic trafficking and neuron-specific sorting of G protein-coupled receptors. J Biol Chem 296:100517. https://doi.org/10.1016/j.jbc.2021.100517
29. Jordan KL, Koss DJ, Outeiro TF, Giorgini F (2022) Therapeutic targeting of Rab GTPases: relevance for Alzheimer's disease. Biomedicines. https://doi.org/10.3390/biomedicines10051141
30. Brewer PD, Habtemichael EN, Romenskaia I, Mastick CC, Coster AC (2016) Glut4 is sorted from a Rab10 GTPase-independent constitutive recycling pathway into a highly insulin-responsive Rab10 GTPase-dependent sequestration pathway after adipocyte differentiation. J Biol Chem 291:773–789. https://doi.org/10.1074/jbc.M115.694919
31. Borchers AC, Langemeyer L, Ungermann C (2021) Who's in control Principles of Rab GTPase activation in endolysosomal membrane trafficking and beyond. J Cell Biol. https://doi.org/10.1083/jcb.202105120
32. Wang P, Liu H, Wang Y, Liu O, Zhang J, Gleason A, Yang Z, Wang H, Shi A, Grant BD (2016) RAB-10 promotes EHBP-1

bridging of filamentous actin and tubular recycling endosomes. PLoS Genet 12:e1006093. https://doi.org/10.1371/journal.pgen.1006093
33. Wan M, Zhang W, Tian Y, Xu C, Xu T, Liu J, Zhang R (2015) Unraveling a molecular determinant for clathrin-independent internalization of the M2 muscarinic acetylcholine receptor. Sci Rep 5:11408. https://doi.org/10.1038/srep11408
34. Schuck S, Gerl MJ, Ang A, Manninen A, Keller P, Mellman I, Simons K (2007) Rab10 is involved in basolateral transport in polarized Madin-Darby canine kidney cells. Traffic 8:47–60. https://doi.org/10.1111/j.1600-0854.2006.00506.x
35. Eguez L, Lee A, Chavez JA, Miinea CP, Kane S, Lienhard GE, McGraw TE (2005) Full intracellular retention of GLUT4 requires AS160 Rab GTPase activating protein. Cell Metab 2:263–272. https://doi.org/10.1016/j.cmet.2005.09.005
36. Tian Y, Kang Q, Shi X, Wang Y, Zhang N, Ye H, Xu Q, Xu T, Zhang R (2021) SNX-3 mediates retromer-independent tubular endosomal recycling by opposing EEA-1-facilitated trafficking. PLoS Genet 17:e1009607. https://doi.org/10.1371/journal.pgen.1009607
37. Volpicelli LA, Lah JJ, Levey AI (2001) Rab5-dependent trafficking of the m4 muscarinic acetylcholine receptor to the plasma membrane, early endosomes, and multivesicular bodies. J Biol Chem 276:47590–47598. https://doi.org/10.1074/jbc.M106535200
38. Krudewig R, Langer B, Vogler O, Markschies N, Erl M, Jakobs KH, van Koppen CJ (2000) Distinct internalization of M2 muscarinic acetylcholine receptors confers selective and long-lasting desensitization of signaling to phospholipase C. J Neurochem 74:1721–1730. https://doi.org/10.1046/j.1471-4159.2000.0741721.x
39. Babbey CM, Ahktar N, Wang E, Chen CC, Grant BD, Dunn KW (2006) Rab10 regulates membrane transport through early endosomes of polarized Madin-Darby canine kidney cells. Mol Biol Cell 17:3156–3175. https://doi.org/10.1091/mbc.e05-08-0799
40. Miinea CP, Sano H, Kane S, Sano E, Fukuda M, Peranen J, Lane WS, Lienhard GE (2005) AS160, the Akt substrate regulating GLUT4 translocation, has a functional Rab GTPase-activating protein domain. Biochem J 391:87–93. https://doi.org/10.1042/BJ20050887
41. Naslavsky N, Caplan S (2018) The enigmatic endosome—sorting the ins and outs of endocytic trafficking. J Cell Sci. https://doi.org/10.1242/jcs.216499
42. Hashimoto Y, Morisawa K, Saito H, Jojima E, Yoshida N, Haga T (2008) Muscarinic M4 receptor recycling requires a motif in the third intracellular loop. J Pharmacol Exp Ther 325:947–953. https://doi.org/10.1124/jpet.107.135095
43. Donaldson JG, Porat-Shliom N, Cohen LA (2009) Clathrin-independent endocytosis: a unique platform for cell signaling and PM remodeling. Cell Signal 21:1–6. https://doi.org/10.1016/j.cellsig.2008.06.020
44. D'Souza-Schorey C, Chavrier P (2006) ARF proteins: roles in membrane traffic and beyond. Nat Rev Mol Cell Biol 7:347–358. https://doi.org/10.1038/nrm1910
45. Houndolo T, Boulay PL, Claing A (2005) G protein-coupled receptor endocytosis in ADP-ribosylation factor 6-depleted cells. J Biol Chem 280:5598–5604. https://doi.org/10.1074/jbc.M411456200
46. Reiner C, Nathanson NM (2008) The internalization of the M2 and M4 muscarinic acetylcholine receptors involves distinct subsets of small G-proteins. Life Sci 82:718–727. https://doi.org/10.1016/j.lfs.2008.01.013
47. D'Souza-Schorey C, van Donselaar E, Hsu VW, Yang C, Stahl PD, Peters PJ (1998) ARF6 targets recycling vesicles to the plasma membrane: insights from an ultrastructural investigation. J Cell Biol 140:603–616. https://doi.org/10.1083/jcb.140.3.603
48. Donaldson JG (2003) Multiple roles for Arf6: sorting, structuring, and signaling at the plasma membrane. J Biol Chem 278:41573–41576. https://doi.org/10.1074/jbc.R300026200
49. Sannerud R, Declerck I, Peric A, Raemaekers T, Menendez G, Zhou L, Veerle B, Coen K, Munck S, De Strooper B, Schiavo G, Annaert W (2011) ADP ribosylation factor 6 (ARF6) controls amyloid precursor protein (APP) processing by mediating the endosomal sorting of BACE1. Proc Natl Acad Sci USA 108:E559-568. https://doi.org/10.1073/pnas.1100745108
50. Van Acker T, Tavernier J, Peelman F (2019) The small GTPase Arf6: an overview of its mechanisms of action and of its role in host(–)pathogen interactions and innate immunity. Int J Mol Sci. https://doi.org/10.3390/ijms20092209
51. Pfeffer SR (2012) Rab GTPase localization and Rab cascades in Golgi transport. Biochem Soc Trans 40:1373–1377. https://doi.org/10.1042/BST20120168
52. Kobayashi H, Fukuda M (2012) Rab35 regulates Arf6 activity through centaurin-β2 (ACAP2) during neurite outgrowth. J Cell Sci 125:2235–2243. https://doi.org/10.1242/jcs.098657
53. Shi A, Liu O, Koenig S, Banerjee R, Chen CC, Eimer S, Grant BD (2012) RAB-10-GTPase-mediated regulation of endosomal phosphatidylinositol-4,5-bisphosphate. Proc Natl Acad Sci USA 109:E2306-2315. https://doi.org/10.1073/pnas.1205278109
54. Allaire PD, Seyed Sadr M, Chaineau M, Seyed Sadr E, Konefal S, Fotouhi M, Maret D, Ritter B, Del Maestro RF, McPherson PS (2013) Interplay between Rab35 and Arf6 controls cargo recycling to coordinate cell adhesion and migration. J Cell Sci 126:722–731. https://doi.org/10.1242/jcs.112375
55. Jackson TR, Brown FD, Nie Z, Miura K, Foroni L, Sun J, Hsu VW, Donaldson JG, Randazzo PA (2000) ACAPs are arf6 GTPase-activating proteins that function in the cell periphery. J Cell Biol 151:627–638. https://doi.org/10.1083/jcb.151.3.627
56. Dai J, Li J, Bos E, Porcionatto M, Premont RT, Bourgoin S, Peters PJ, Hsu VW (2004) ACAP1 promotes endocytic recycling by recognizing recycling sorting signals. Dev Cell 7:771–776. https://doi.org/10.1016/j.devcel.2004.10.002
57. Takatsu H, Yoshino K, Toda K, Nakayama K (2002) GGA proteins associate with Golgi membranes through interaction between their GGAH domains and ADP-ribosylation factors. Biochem J 365:369–378. https://doi.org/10.1042/BJ20020428
58. Carroll RC, Morielli AD, Peralta EG (1995) Coincidence detection at the level of phospholipase C activation mediated by the m4 muscarinic acetylcholine receptor. Curr Biol 5:536–544. https://doi.org/10.1016/s0960-9822(95)00106-0
59. Esseltine JL, Ribeiro FM, Ferguson SS (2012) Rab8 modulates metabotropic glutamate receptor subtype 1 intracellular trafficking and signaling in a protein kinase C-dependent manner. J Neurosci 32:16933–16942a. https://doi.org/10.1523/JNEUROSCI.0625-12.2012
60. Richards MH, van Giersbergen PL (1995) Human muscarinic receptors expressed in A9L and CHO cells: activation by full and partial agonists. Br J Pharmacol 114:1241–1249. https://doi.org/10.1111/j.1476-5381.1995.tb13339.x
61. Li C, Wei Z, Fan Y, Huang W, Su Y, Li H, Dong Z, Fukuda M, Khater M, Wu G (2017) The GTPase Rab43 controls the anterograde ER-Golgi trafficking and sorting of GPCRs. Cell Rep 21:1089–1101. https://doi.org/10.1016/j.celrep.2017.10.011
62. Dong C, Yang L, Zhang X, Gu H, Lam ML, Claycomb WC, Xia H, Wu G (2010) Rab8 interacts with distinct motifs in alpha2B- and beta2-adrenergic receptors and differentially modulates their transport. J Biol Chem 285:20369–20380. https://doi.org/10.1074/jbc.M109.081521

63. Seachrist JL, Laporte SA, Dale LB, Babwah AV, Caron MG, Anborgh PH, Ferguson SS (2002) Rab5 association with the angiotensin II type 1A receptor promotes Rab5 GTP binding and vesicular fusion. J Biol Chem 277:679–685. https://doi.org/10.1074/jbc.M109022200
64. Chen CC, Schweinsberg PJ, Vashist S, Mareiniss DP, Lambie EJ, Grant BD (2006) RAB-10 is required for endocytic recycling in the *Caenorhabditis elegans* intestine. Mol Biol Cell 17:1286–1297. https://doi.org/10.1091/mbc.e05-08-0787
65. Chen S, Li L, Li J, Liu B, Zhu X, Zheng L, Zhang R, Xu T (2014) SEC-10 and RAB-10 coordinate basolateral recycling of clathrin-independent cargo through endosomal tubules in *Caenorhabditis elegans*. Proc Natl Acad Sci USA 111:15432–15437. https://doi.org/10.1073/pnas.1408327111
66. Mulvaney EP, O'Meara F, Khan AR, O'Connell DJ, Kinsella BT (2017) Identification of alpha-helix 4 (alpha4) of Rab11a as a novel Rab11-binding domain (RBD): interaction of Rab11a with the prostacyclin receptor. Biochim Biophys Acta Mol Cell Res 1864:1819–1832. https://doi.org/10.1016/j.bbamcr.2017.07.010
67. Tanna CE, Goss LB, Ludwig CG, Chen PW (2019) Arf GAPs as regulators of the actin cytoskeleton-an update. Int J Mol Sci. https://doi.org/10.3390/ijms20020442
68. Pfeffer SR (2017) Rab GTPases: master regulators that establish the secretory and endocytic pathways. Mol Biol Cell 28:712–715. https://doi.org/10.1091/mbc.E16-10-0737
69. Donaldson JG, Johnson DL, Dutta D (2016) Rab and Arf G proteins in endosomal trafficking and cell surface homeostasis. Small GTPases 7:247–251. https://doi.org/10.1080/21541248.2016.1212687
70. Fielding AB, Schonteich E, Matheson J, Wilson G, Yu X, Hickson GR, Srivastava S, Baldwin SA, Prekeris R, Gould GW (2005) Rab11-FIP3 and FIP4 interact with Arf6 and the exocyst to control membrane traffic in cytokinesis. EMBO J 24:3389–3399. https://doi.org/10.1038/sj.emboj.7600803
71. Kiral FR, Kohrs FE, Jin EJ, Hiesinger PR (2018) Rab GTPases and membrane trafficking in neurodegeneration. Curr Biol 28:R471–R486. https://doi.org/10.1016/j.cub.2018.02.010
72. Zhang X, Huang TY, Yancey J, Luo H, Zhang YW (2019) Role of Rab GTPases in Alzheimer's disease. ACS Chem Neurosci 10:828–838. https://doi.org/10.1021/acschemneuro.8b00387